Short title: Two isoforms of AtSCS

Correspondence to: Maria Bucholc and Grażyna Dobrowolska
Institute of Biochemistry and Biophysics, Polish Academy of Sciences,
Pawińskiego 5a, 02-106 Warsaw, Poland
Tel: 48-22-5925715
Fax: 48-22-6584636
e-mail: mjb@ibb.waw.pl; dobrowol@ibb.waw.pl

Article title: Biochemical, Biophysical, and Functional Analyses of Two Isoforms of the SnRK2 inhibitor AtSCS

Authors: Krzysztof Tarnowski[1#], Maria Klimecka[1#], Arkadiusz Ciesielski[1,2], Grażyna Goch[1], Anna Kulik[1], Halina Fedak[1], Jarosław Poznański[1], Małgorzata Lichocka[1], Marcin Pierechod[3¶], Richard A. Engh[3], Michał Dadlez[1,4], Grażyna Dobrowolska[1*], Maria Bucholc[1*]

Affiliations:

[1] Institute of Biochemistry and Biophysics, Polish Academy of Sciences, Pawińskiego 5a, 02-106 Warsaw, Poland

[2] Warsaw University, Department of Chemistry, Pasteura 1, 02-093 Warsaw, Poland

[3] The Norwegian Center for Structure Biology, Institute of Chemistry, University of Tromsø, N-9037 Tromsø, Norway

[4] University of Warsaw, Institute of Genetics and Biotechnology, Pawińskiego 5a, 02-106 Warsaw, Poland

One sentence Summary: Two isoforms of SnRK2-interacting calcium sensor are expressed in Arabidopsis; they differ in calcium binding properties, but both of them inhibit SnRK2s and subsequently fine tune ABA signaling.

Footnotes

M.B., G.D., M.D., and R.A.E. supervised the experiments; K.T., M.K., M.B., A.C., G.G., H.F., J.P., M.L., A.K., M.P. performed the experiments; M.B., G.D., M.K., K.T., G.G., J.P. designed the experiments and analyzed the data; G.D., M.B., M.K., R.A.E.

conceived the project and wrote the article with contributions of all the authors. G.D. supervised and complemented the writing.

[#] These authors contribute equally to the work.

[¶] present address: Norwegian Ice Service, Norwegian Meteorological Institute, Kirkegårdsveien 60, NO-9023 Tromsø, Norway

This work was supported by the Norwegian Research Council and the Research Program of the EEA/Norway Grants (grant PolNor/203156/70/2013 to GD and RAE), National Science Centre (grants: 2011/01/B/NZ3/02899 to MB, 2016/23/B/NZ3/03182 to GD, 2014/13/D/NZ3/03101 to AK, MAESTRO 2014/14/A/NZ1/00306 to MD, and Centre of Preclinical Research and Technology (POIG.02.02.00–14–024/08-00), National Multidisciplinary Laboratory of Functional Nanomaterials (POIGT.02.02.00-00-025/09-00).

* Corresponding authors: Maria Bucholc and Grażyna Dobrowolska

e-mail: mjb@gmail.; dobrowol@ibb.waw.pl

ABSTRACT

SNF1-related protein kinases 2 (SnRK2s) are key signaling elements that regulate abscisic acid (ABA)-dependent plant development and responses to environmental stresses. Our previous data showed that the SnRK2-interacting Calcium Sensor (SCS) is an inhibitor of SnRK2 activity. In *Arabidopsis thaliana,* the use of alternative transcription start sites located within *AtSCS* gene results in two in-frame transcripts and subsequently two proteins, which differ only by the sequence position of the N-terminus. We described the longer AtSCS-A earlier, and now we describe the shorter AtSCS-B and compare both isoforms. The two forms differ significantly in their expression profiles in plant organs and in response to environmental stresses, in calcium binding properties, and conformational dynamics in the presence and absence of Ca^{2+}. The results show that only AtSCS-A has the features of a calcium sensor. Both forms inhibit SnRK2 activity, but differ with respect to calcium dependence, as AtSCS-A requires calcium for inhibition, while AtSCS-B does not. Analysis of Arabidopsis plants stably expressing *35S::AtSCS-A-c-myc* or *35S::AtSCS-B-c-myc* in the *scs-1* knockout mutant revealed that *in planta* both forms are negative regulators of the SnRK2 activity induced in response to ABA and regulate plant defense against water deficit. Moreover, the data present biochemical, biophysical, and functional properties of EF-hand-like motifs in plant proteins.

INTRODUCTION

SNF1-related protein kinases 2 (SnRK2s) are plant specific kinases involved in plant response to environmental stresses (e.g., water deficit, salinity) and in abscisic acid (ABA)-dependent development (for reviews see: Hubbard et al., 2010; Fujita et al., 2011; Kulik et al., 2011; Nakashima and Yamaguchi-Shinozaki, 2013; Yoshida et al., 2015). Based on phylogenetic analyses, SnRK2s have been classified into three groups. The classification correlates closely with their sensitivity to ABA; group 1 consists of SnRK2s which are not activated by ABA treatment, group 2 includes kinases which are not or only weakly activated by ABA, and group 3 kinases are strongly activated by the phytohormone. Ample data demonstrate the role of group 3 SnRK2s in ABA signaling, both in plant development as well as in stress response. In *Arabidopsis thaliana,* group 3 comprises three members: SnRK2.2, SnRK2.3 and SnRK2.6. SnRK2.2 and SnRK2.3 are involved mainly in the regulation of seed

dormancy and germination (Fujii *et al.*, 2007), whereas SnRK2.6 regulates stomatal closure in response to water deficit, pathogen infection, CO_2, ozone, and darkness (Mustilli et al., 2002; Yoshida et al., 2002; Melotto et al., 2006; Merilo et al., 2013). However, there is significant functional redundancy between the three kinases. The Arabidopsis triple knockout mutant *snrk2.2/snrk2.3/snrk2.6* is extremely insensitive to ABA (much more than the single or double knockout mutants), exhibits severely impaired seed development and dormancy, and is oversensitive to water scarcity due to disruption of stomatal closure and down-regulation of ABA- and water stress-induced genes (Fujii and Zhu, 2009; Fujita et al., 2009; Nakashima et al., 2009). SnRK2s, which are either not or only weakly activated in response to ABA, are also involved in regulation of plant responses to abiotic stresses (Umezawa et al., 2004; Mizoguchi et al., 2010; Fujii et al., 2011; McLoughlin et al., 2012; Kulik et al., 2012; Soma et al., 2017).

The SnRK2 kinases are activated transiently in plant cells in response to environmental signals, and otherwise are maintained in inactive states. The best-known negative regulators of SnRK2s are protein phosphatases (Umezawa et al., 2009; Vlad et al., 2009; Hou et al., 2016; Krzywińska et al., 2016). Clade A phosphoprotein phosphatases 2C (PP2Cs) have been identified as major regulators of ABA-activated SnRK2s (Umezawa et al., 2009; Vlad et al., 2009; and reviews: Hubbard et al., 2010; Fujita et al., 2011; Nakashima and Yamaguchi-Shinozaki, 2013; Yoshida et al., 2015). Functional and structural studies showed that PP2Cs hold SnRK2s in an inactive state via a two-step inhibition mechanism (Soon et al., 2012; Zhou et al., 2012; Ng et al., 2014): specific Ser/Thr residues in the kinase activation loop are dephosphorylated, and a physical interaction between the kinase activation loop and the phosphatase active site persists to additionally block the kinase activity. Those results suggested that activity modulation is controlled not only by the phosphorylation state of SnRK2s but also by specific protein-protein interactions.

A few years ago, we identified and partially characterized another inhibitor of SnRK2 kinases and consequently of ABA signaling, SnRK2-interacting Calcium Sensor (SCS) (Bucholc et al., 2011). SCS provides the link between SnRK2s and calcium signaling pathways.

Calcium ions are ubiquitous second messengers that play pivotal roles in plant response to a number of external signals, inducing and regulating plant development,

and responding to biotic and abiotic stresses. Several hundreds of plant proteins that potentially bind calcium have been identified; it was estimated that the Arabidopsis genome encodes about 250 EF-hand- or putative EF-hand-containing proteins (Day et al., 2002; Reddy and Reddy, 2004). Arabidopsis, presumably along with other plants, contain many more proteins with canonical and non-canonical EF-hand ("EF-hand-like") motifs than other organisms. In plants, non-canonical EF-hand motifs are especially abundant (Day et al., 2002). Only a small fraction of them has been characterized. Numerous proteins with putative EF-hand-like motifs are involved in signal transduction; most probably they evolved to sense different calcium levels. Many of them contain four EF-hand sequences, with variable degrees of conservation of canonical EF-hand calcium binding motifs. This group comprises both sensor responder proteins (activated directly upon calcium binding and transmitting the signal further), as well as sensor relay proteins, which do not have enzymatic activity; upon Ca^{2+} binding, they undergo conformational changes and trigger activation or deactivation of their cellular partners. The best examples of sensor responder proteins are calcium dependent protein kinases (CDPKs), usually with four calmodulin-like EF-hand motifs and a Ser/Thr protein kinase domain that is activated upon calcium binding (review: Schulz et al., 2013). Sensor relay proteins involved in plant signaling constitute two main families: calmodulins (CaMs) and calcineurin B-like (CBL) proteins. Like CDPKs, each of them has four EF-hand or EF-hand-like motifs. Some CBLs harbor one or two canonical EF-hand motifs; most, however, have only EF-hand-like motifs (Batistič and Kudla, 2009; Sanchez-Barrena et al., 2013). The variety in calcium binding motif sequences determines the diversity in sensor proteins needed for sensing various calcium signatures, and finally to achieve the response specificity. However, for most CBLs and other predicted calcium binding proteins the actual calcium binding properties have not been characterized.

SCSs share several similar features with CBL proteins. According to the Prosite prediction of properties based on sequence, the *Arabidopsis thaliana* SCS protein (At4g38810) described by us earlier (Bucholc et al., 2011) contains four peptide sequences resembling EF-hand motifs, of which only one possesses all residues that define a canonical EF-hand. The other three are quite distinctly non-canonical and may be considered EF-hand-like. Also like CBLs, SCS is sensor relay protein involved in signal transduction in plants via interactions with SNF1-related protein

158 kinases (SnRKs), unique to the plant kingdom. While SCSs interact with SnRK2s,
159 CBLs interact with the SnRK3 kinases, also known as CBL-interacting protein
160 kinases (CIPKs) or protein kinases related to SOS2 (PKSs). Both CBLs and SCSs
161 regulate kinase activity, but in opposite ways, as CBLs activate CIPKs (for review see
162 Batistič and Kudla, 2009; Luan, 2009; Batistič and Kudla, 2012) whereas SCSs
163 inhibit SnRK2s.

164 Information provided by The Arabidopsis Information Resource (TAIR) indicates
165 that in Arabidopsis two forms of AtSCS may exist, a longer one with 375 aa (denoted
166 here as AtSCS-A, as described previously (Bucholc et al., 2011), and its shorter
167 version with 265 aa (AtSCS-B) corresponding to the 111-375 aa fragment of AtSCS-
168 A, in which the classical EF-hand motif is missing (Fig. 1A and 1B). *In silico* analysis
169 of the *AtSCS* gene (At4g38810) sequence indicates that expression of both forms is
170 possible due to the alternative transcription start sites (TSS); one promoter region is
171 located upstream of ATG codon of *AtSCS-A*, and the second one responsible for
172 *AtSCS-B* transcription within first *AtSCS-A* intron (Fig 1A). Alternative mRNA
173 transcription starting, like alternative mRNA processing, is a well known regulatory
174 process in eukaryotic organisms, including plants, which expands the genome's
175 coding capacity and generates protein variation (Tanaka et al., 2009; de Klerk and 't
176 Hoen, 2015). The result of alternative TSS are usually isoforms of proteins, which
177 differ in their function, stability, localization and/or expression levels.

178 In the present studies we confirmed the expression of both forms of AtSCS in
179 Arabidopsis and showed significant differences in their expression profiles in plant
180 organs and in response to abiotic stress. We compared both proteins with respect to
181 Ca^{2+}-binding properties, conformational dynamics with and without Ca^{2+}, and
182 regulation of the kinase activity *in vitro* and *in vivo*. Analysis of transgenic plants
183 expressing *35S::AtSCS-A-c-myc* or *35S::AtSCS-B-c-myc* in the *scs-1* knockout
184 background showed that both forms inhibit the ABA-responsive SnRK2s and, as a
185 consequence, ABA signaling. The results show that both isoforms play a role in the
186 regulation of the plant response to dehydration, analogous to that of the A-clade
187 PP2Cs. Moreover, our results provide novel biochemical and biophysical data on EF-
188 hand–like motifs in plant proteins.

189

190

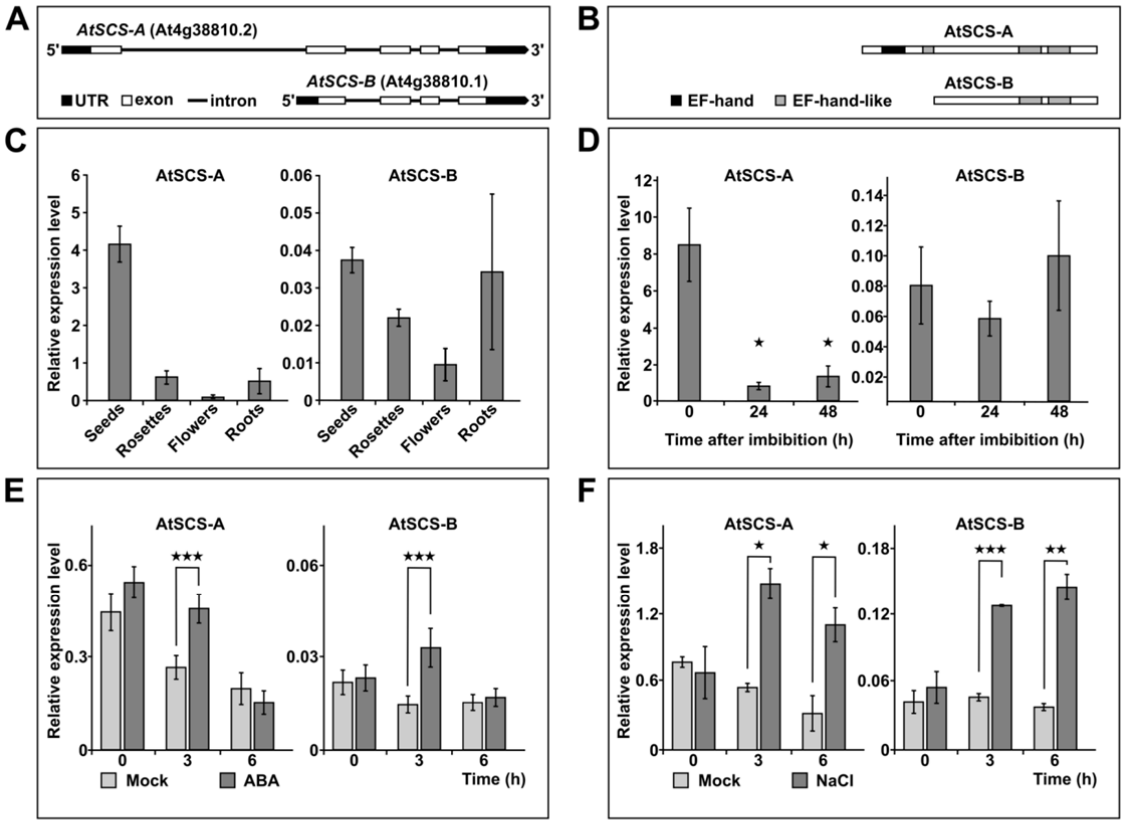

Figure 1.
The expression of AtSCS-A and AtSCS-B varies across plant organs and in plant response to ABA or NaCl treatment. Alternative isoforms of AtSCS (At4g38810), AtSCS-A and AtSCS-B, predicted at transcript (A) and protein (B) levels. The prediction was done based on TAIR plant promoter database (PlantPromoterDB) and Prosite (prediction of EF-hand motifs).
Quantitative RT-PCR analysis of AtSCS-A and AtSCS-B transcript levels in different organs (C), in seeds during germination (D), in 2-week-old seedlings exposed to 10 μM ABA (E) or 150 mM NaCl (F). In E and F - expression levels in plants exposed to ABA or NaCl (dark grey), whereas in control plants, mock treatment (light grey). Data represent means of triplicate biological repeats, and the error bars indicate SD. For statistical analysis a two-tailed t-test in Microsoft Office Excel was applied. The asterisks indicate significant difference from the wild type (*P < 0.05; **P < 0.01, ***P < 0.001).

RESULTS

AtSCS-A and AtSCS-B are Differently Expressed in Plant Tissues and in Arabidopsis Seedlings Subjected to ABA or Salt Stress

To verify that two forms of AtSCS are expressed in Arabidopsis, we analyzed mRNA level of *AtSCS-A* and *AtSCS-B* in various plant organs (seeds, rosettes, flowers, and roots). Moreover, since the functional analysis of AtSCS done previously by a reverse genetic approach indicated that AtSCS is involved in ABA signaling (Bucholc et al., 2011), we monitored *AtSCS-A* and *AtSCS-B* expression in seedlings

exposed to ABA (10 μM) or salt stress (150 mM NaCl). To eliminate the potential influence of the circadian clock on the transcript levels, at each time point the transcript level of *AtSCS-A* and *AtSCS-B* was also monitored in plants not exposed to the stressor or ABA. The highest level of *AtSCS-A* transcript was observed in dry seeds, and the lowest in flowers (Fig. 1C and Supplemental Fig. S1). *AtSCS-B* expression was the highest in seeds and in roots, however, as it is shown in Fig. 1C and Fig. S1 *AtSCS-B* was expressed at a much lower level than *AtSCS-A* in all organs studied; in dry seeds expression of *AtSCS-A* was about 100 times higher than that of *AtSCS-B.* During seed imbibition the transcript level of *AtSCS-A* rapidly declined; after 24 h of imbibition the expression was about 10 times lower than that in dry seeds; in contrast, the transcript level of *AtSCS-B* did not change significantly during imbibition (Fig. 1D).

Analysis of *AtSCS-A* and *AtSCS-B* expression in seedlings exposed to 10 μM ABA showed transient increases (1.7- and 2.3-fold, respectively, at 3 hours) over levels in seedlings not exposed to ABA, with the differences disappearing by 6 hours after treatment (Fig. 1E). Salinity stress (150 mM NaCl) increased expression levels persistently (observed at both 3 and 6 h after treatment), to levels about 3 to 4-fold higher for both isoforms (Fig. 1F). It should be noted that only AtSCS-A expression undergoes changes during diurnal rhythm.

AtSCS-B Interacts with Members of Group 2 and 3 of the SnRK2 Family

To determine whether AtSCS-B, like AtSCS-A, interacts with SnRK2s, we used a yeast two-hybrid approach. cDNA encoding AtSCS-B was fused in-frame to cDNA encoding the Gal4 activation domain in pGAD424 yeast expression vector, and cDNA encoding each of SnRK2s studied was fused to the Gal4 DNA-binding domain in pGBT9 vector. Using parallel constructions, we also studied interactions between AtSCS-A and SnRK2s. Those can be considered to be positive controls, since interactions between SnRK2s and AtSCS-A have been established previously (Bucholc et al., 2011). The results revealed that AtSCS-B interacts with SnRK2s from group 3 (SnRK2.2, SnRK2.3, and SnRK2.6) and from group 2 (SnRK2.7 and SnRK2.8), but does not interact with ABA-non-activated SnRK2 kinases from group 1 (SnRK2.1, SnRK2.4, SnRK2.5 and SnRK2.10) or with SnRK2.9 (Fig. 2A). The results suggest that AtSCS-B is a cellular regulator of members of groups 2 and 3 but not

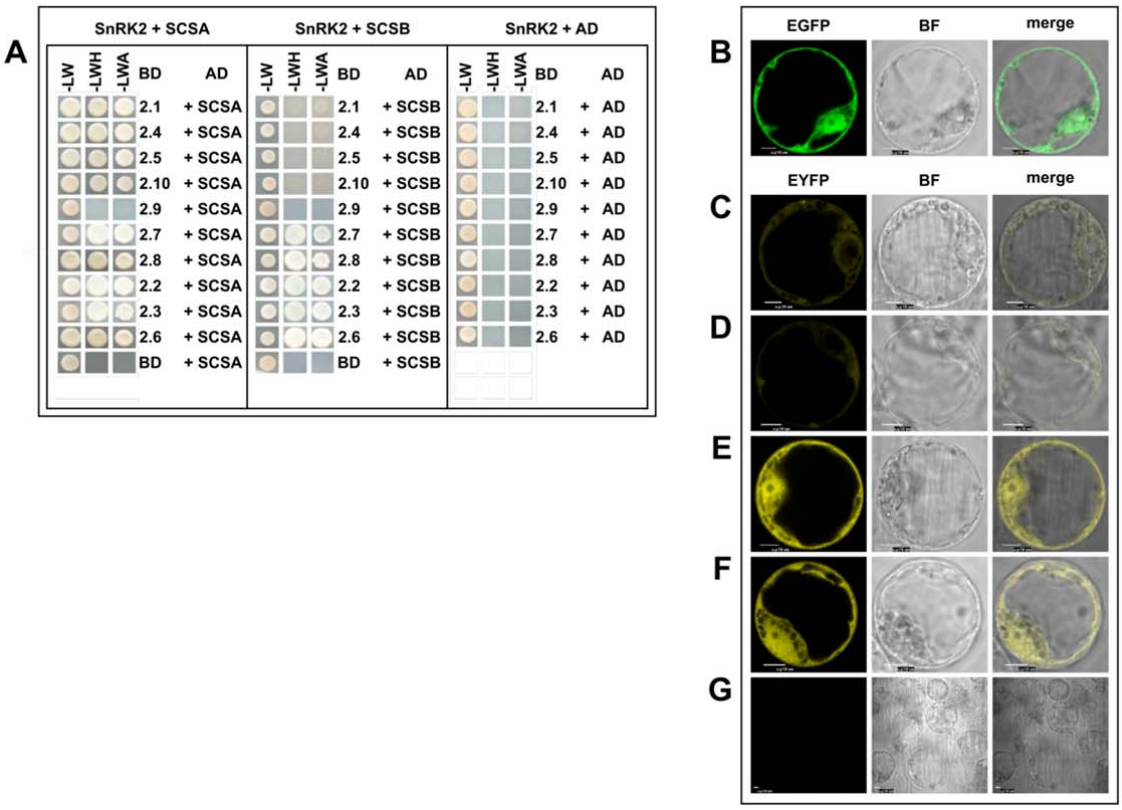

Figure 2.
AtSCS-B interacts preferentially with kinases that belong to group 2 and 3 of the SnRK2 family. Interactions between Arabidopsis SnRK2s and AtSCS-B, or AtSCS-A as a control, were analyzed by a yeast two-hybrid assay (A), as described in Bucholc et al., 2011. Yeast transformed with a construct with cDNA encoding one of the analyzed SnRK2s and complementary empty vector (BD-SnRK2+AD), or a construct with AtSCS-B or AtSCS-A and the other empty vector (BD+AD-AtSCS) were used as controls. The growth of yeast expressing the indicated constructs was monitored on selective media: without Leu and Trp (-LW); without Leu, Trp and His and with 8mM AT (-LWH); without Leu, Trp and Ade (–LWA). AD, Gal4 activation domain; BD, Gal4 binding domain.
The subcellular localization of AtSCS-B was analyzed in Arabidopsis protoplasts (B), as described in Bucholc et al., 2011. Protoplasts isolated from the T87 Arabidopsis cell line were transiently transformed with plasmid encoding AtSCS-B-EGFP and its localization was analyzed by confocal microscopy.
Interaction between AtSCS-B and SnRK2s in planta was analyzed by BiFC assay. T87 protoplasts were transiently co-transformed with pairs of plasmids encoding: AtSCS-B-cEYFP and nEYFP-SnRK2.4 (C), AtSCS-B-cEYFP and nEYFP-SnRK2.10 (D), AtSCS-B-cEYFP and nEYFP-SnRK2.6 (E), AtSCS-B-cEYFP and nEYFP-SnRK2.8 (F). The binding led to reconstitution of functional YFP from chimeric proteins bearing non-florescent halves of YFP. For negative control, AtSCS-B-cEYFP was co-expressed with AtSCS-B-nEYFP (G). Scale bar = 10 μm; BF, bright field. The data shown here represent one of three independent experiments, all with similar results.

group 1 of the SnRK2 family. In contrast, AtSCS-A does not discriminate between these kinases in respect to the interaction. The only Arabidopsis SnRK2 that does not bind to either form of AtSCS is SnRK2.9.

The interactions between AtSCS-B and the selected SnRK2s were verified by bimolecular fluorescence complementation (BiFC) assays. The proteins were

expressed in Arabidopsis protoplasts as described in Bucholc et al. (2011). First, we analyzed the subcellular localization of AtSCS-B. The protein was produced as a fusion with EGFP using the pSAT6-EGFP-N1 or pSAT6-EGFP-C1 vector. As with AtSCS-A (Bucholc et al., 2011), AtSCS-B localized to the nucleus and cytoplasm (Fig. 2B). In a BiFC assay we analyzed interactions between AtSCS-B and SnRK2.4, SnRK2.10, SnRK2.6, and SnRK2.8 (Fig. 2C-2F). The kinases and AtSCS-B were each fused to complementary non-fluorescent fragments of YFP and transiently produced in Arabidopsis protoplasts. The BiFC assays showed that SnRK2.6 (from group 3) and SnRK2.8 (from group 2) interact with the AtSCS-B *in planta*. The interactions occur both in the cytoplasm and nucleus. SnRK2.4 and SnRK2.10 (from group 1) did not interact with AtSCS-B (in agreement with two-hybrid assay) or they interact very weakly, as the YFP signal is much weaker for these two kinases than that observed for SnRK2.6 or SnRK2.8. This supports the view that AtSCS-B is rather not a cellular regulator of ABA-non-activated SnRK2 kinases. A very low fluorescence signal detectable in the negative control samples was much weaker than YFP signal in BiFC samples (Fig. 2G). A comparison with AtSCS-A should be noted; as published previously, AtSCS-A interacts with all SnRK2 kinases studied, but exclusively in the cytoplasm (Bucholc et al., 2011).

AtSCS-B Inhibits SnRK2 Activity in Calcium-Independent Manner

Our previous results showed that AtSCS-A inhibits SnRK2 activity only in the presence of calcium ions (Bucholc et al., 2011). To check whether AtSCS-B inhibition of SnRK2 activity is similarly calcium dependent we monitored the *in vitro* activity of SnRK2.6 and SnRK2.8 in the presence of increasing amounts of purified recombinant AtSCS-B, with and without calcium ions in the reaction mixture. The kinase activity was analyzed using MBP as a substrate. The results showed that AtSCS-B, in contrast to AtSCS-A, inhibits the SnRK2 activity both in the presence and in the absence of calcium ions (in the presence of EGTA) (Fig. 3A and 3B).

Both AtSCS-A and AtSCS-B Inhibit the SnRK2 Activity *in planta*

To investigate the involvement of AtSCS-A and AtSCS-B in the regulation of SnRK2 activity *in vivo* we obtained homozygous transgenic Col-0 Arabidopsis plants

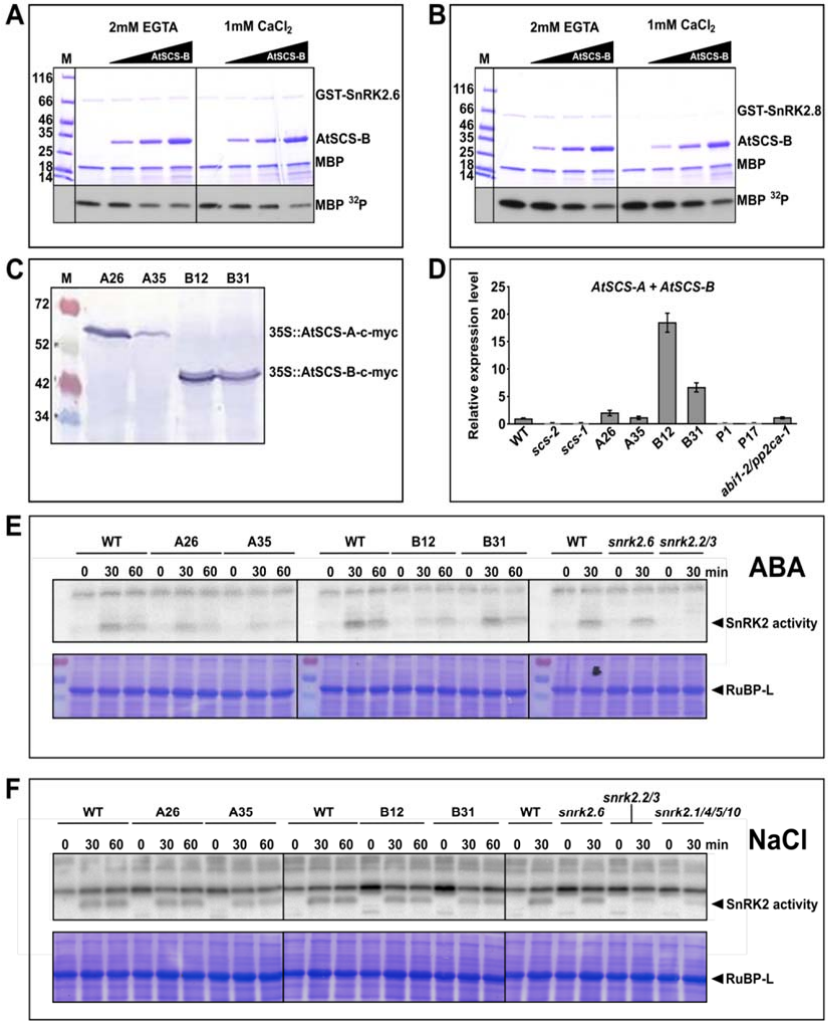

Figure 3.

AtSCS-A and AtSCS-B inhibit the SnRK2 activity in vitro and in vivo. AtSCS-B inhibition of SnRK2.6 (A) and SnRK2.8 (B) is calcium independent. SnRK2.6, SnRK2.8, and AtSCS-B were expressed in *E.coli* and the kinase activity was measured in the presence of increasing amounts of AtSCS-B (0, 40, 80 and 160 ng per µL) without or with Ca^{2+} (2 mM EGTA or 1 mM $CaCl_2$, respectively) in the reaction mixture. The kinase activity was monitored using MBP and [γ^{32}P]ATP as substrates. Reaction products were separated by SDS-PAGE and MBP phosphorylation was determined by autoradiography. The data represent one of three independent experiments showing similar results.

The expression of AtSCS-A and AtSCS-B in seedlings of homozygous transgenic lines 35S::AtSCS-A-c-myc (A26 and A35) and 35S::AtSCS-B-c-myc (B12 and B31) was measured at protein (C) and transcript (D) levels. The production of AtSCS-A-c-myc and AtSCS-B-c-myc proteins was monitored in seedlings of the transgenic plants by Western blotting using anti-c-myc antibodies. *AtSCS* mRNA level was monitored in the transgenic plants expressing *AtSCS-A-c-myc* or *AtSCS-B-c-myc*, or *c-myc* (vector control: P1, P17), the *scs-1* and *scs-2* mutants, as well in the WT plants by quantitative RT-PCR analysis. Data represent means of triplicate biological repeats, and the error bars indicate SD.

Analysis of the SnRK2 activity in 2-week-old seedlings of the WT, transgenic plants expressing *AtSCS-A-c-myc* or *AtSCS-B-c-myc*, and selected *snrk2* knockout mutants subjected to 100 µM ABA (E) or 350 mM NaCl (F) shows significant *in planta* inhibition by AtSCS isoforms. The kinase activity was monitored by in-gel-kinase activity assay using as substrate GST-ABF2 (G73-Q120) or MBP, respectively. The representative results from one of three independent experiments are shown.

274 expressing *AtSCS-A-c-myc* (5 independent lines) or *AtSCS-B-c-myc* (3 independent

lines) under control of the 35S promoter, as well as plants expressing an empty vector, in an *scs-1* knockout background deficient in both AtSCS forms. For the studies we selected two transgenic lines 35S::AtSCS-A-c-myc (A26 and A35), 35S::AtSCS-B-c-myc (B12 and B31), with the highest expression of the transgene (Fig. 3C, 3D, and Supplemental Fig. S2). We analyzed the kinase activity phosphorylating ABF2 (Gly73-Gln120) peptide (in the case of plants exposed to ABA) or myelin basic protein (MBP, in the case of plants exposed to NaCl) in 2-week-old seedlings of A26, A35, B12, and B31 lines, and the wild type Arabidopsis (WT). The activity was analyzed before and after treatment with 100 μM ABA (or 350 mM NaCl) by in-gel kinase activity assay according to Wang and Zhu (2016). The SnRK2 activity induced in response to ABA was significantly lower in both 35S::AtSCS-A-c-myc lines (A26 and A35) and in one of 35S::AtSCS-B-c-myc lines (B12) compared to WT plants (Fig. 3E). In the B31 line, with its lower expression of AtSCS-B-c-myc compared to B12 line, the ABA-induced SnRK2 activity was similar to that observed in the WT plants. These results indicate that both AtSCS-A and AtSCS-B inhibit the kinase activity induced by ABA treatment; however, the inhibition is stronger in the presence of AtSCS-A. The analysis of the kinase activity in the same Arabidopsis lines treated with NaCl showed only very weak, if any, inhibition of the SnRK2 activity by AtSCSs (Fig 3F). In summary, these results indicate that both forms of AtSCS are able to inhibit the SnRK2s *in vivo*, especially those kinases which are involved in ABA signaling.

AtSCS-A and AtSCS-B Have an Impact on the Plant Sensitivity to Dehydration

Our results showed that expression of *AtSCS-A* and *AtSCS–B* is induced in the response to ABA (Fig.1E). Moreover, the activity of ABA-responsive kinases in Arabidopsis seedlings overexpressing AtSCS-A or AtSCS-B exposed to exogenous ABA is significantly reduced in comparison to that observed in the WT plants (Fig. 3E). Since the ABA-responsive SnRK2s are key regulators of the plant response to dehydration, we studied the impact of AtSCSs on the plant response to water deficit. We analyzed the survival rate of the Col-0 WT, the *scs* knockout mutants (lines *scs-2* and vector control P1, 35S:c-myc in *scs-1* background), 35S::AtSCS-A-c-myc (A26 and A35 lines) and 35S::AtSCS-B-c-myc (B12 and B31lines) transgenic plants under drought conditions (the watering was withdrawn for 14 days) and after re-watering. In

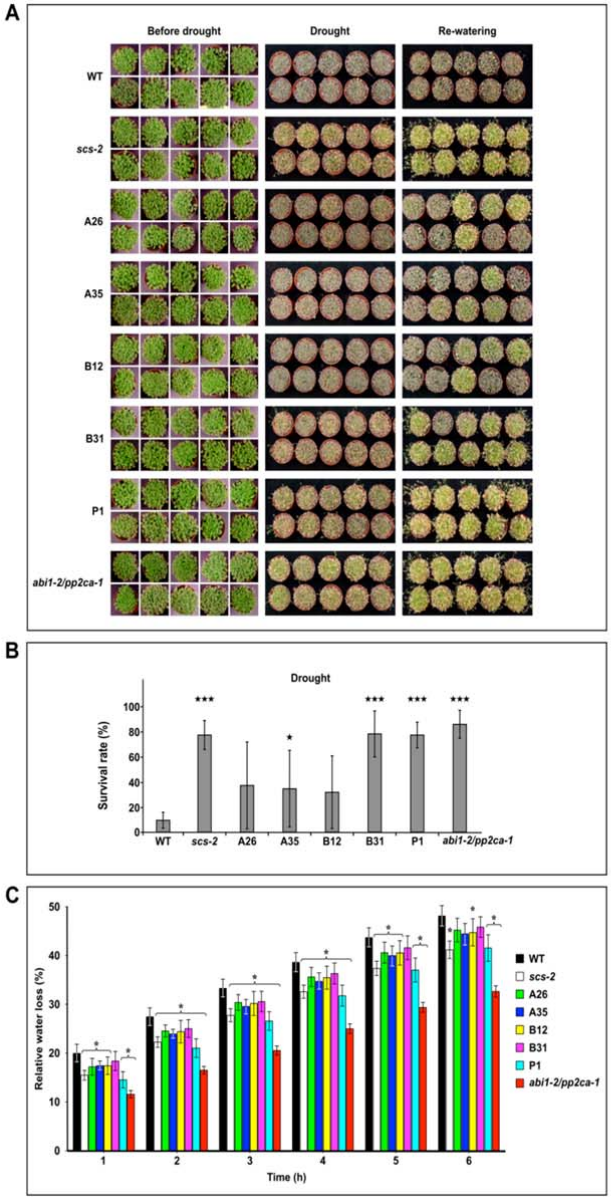

Figure 4.

AtSCS-A and AtSCS-B Regulate the Response of Arabidopsis to Water Deficit. The drought survival rate test (A). The Arabidopsis plants were grown in pots for 17 days under long day conditions and for an additional 2 weeks without watering. The pictures were taken before watering was stopped (before drought), after two weeks without water (drought), and two days after re-watering (re-watering). Ten pots with approximately 50 plants for each line per experiment were used. Representative plants are presented. The drought survival rate (B) was calculated by analysis of at least 1000 plants per each line. For the statistical analysis a t-test was applied. The asterisks indicate significant differences from the wild type (*P < 0.05; **P < 0.01, ***P < 0.001). The average values ± SE are shown.

Water loss from detached Arabidopsis rosettes (C). Rates of water loss from the whole rosettes of six-week-old plants of wild type and different mutant lines were measured at the time points indicated. Finally, the rosettes were dried at 70°C overnight and weighed. The cut rosette water loss (CRWL) was calculated. The representative results from one of four independent experiments are shown. Eight plants were used for each line per experiment. For the statistical analysis, a t-test was applied. The asterisks indicate significant differences from the wild type (*P < 0.05; **P < 0.01, ***P < 0.001). The average values ± SE are shown.

309 our assay we also included an *abi1-2/pp2ca-1* mutant deficient in two clade A PP2C

phosphates, ABI1 and PP2CA, well known inhibitors of ABA-dependent SnRK2s and ABA signaling (Umezawa et al., 2009; Vlad et al., 2009; Rubio et al., 2009), as a control. Our results confirmed previously published data (Rubio et al., 2009) that the *abi1-2/pp2ca-1* mutant exhibits enhanced resistance to drought stress and showed that the *scs-2* mutant and P1 line similarly as *abi1-2/pp2ca-1* were more resistant to dehydration than all other lines studied (Fig. 4A and 4B). The data indicated similar regulation of the response to dehydration of AtSCSs and the clade A PP2Cs. The results also showed that expression of *AtSCS-A* (lines A26 and A35) or *AtSCS-B* (especially line B12 with a higher level of AtSCS-B) alone only partially complement the phenotype of the *scs* mutant, which suggests that both forms of SCS are needed for the full complementation.

Additionally, we measured water loss in detached rosettes of 6-week-old plants of all the lines listed above. The water loss was lower in rosettes of the *scs* mutants (*scs2* and P1, vector control in *scs1* background) than in other lines (Fig. 4C), which is in agreement with the result of drought survival test (Fig. 4A and 4B).

Using Arabidopsis lines with differing the AtSCS-A or AtSCS-B levels we also investigated the involvement of AtSCSs in regulation of the expression of ABA-induced stress-related genes. For the analysis we chose two genes regulated by SnRK2s in an ABA-dependent manner, *Rab18* and *RD29B*. We did not observe any significant differences in the expression of genes studied in response to ABA between lines studied (Supplemental Fig S3) indicating that SCSs are rather not involved in the regulation of gene expression. This result is consistent with our data showing that SCSs interact with SnRK2s mainly in the cytoplasm; AtSCS-A interacts exclusively in the cytoplasm (Bucholc et al., 2011, Fig.2B), whereas AtSCS-B in the cytoplasm and in the nucleus. However, we cannot exclude the possibility that transiently overexpressed AtSCS-B-GFP/YFP is passively diffused to the nucleus (that is why we observe its presence both in the cytoplasm and the nucleus).

AtSCS-B Binds Ca^{2+} Without a Substantial Effect on the Protein Conformation

In order to compare calcium-binding properties of AtSCS-B to that of AtSCS-A described earlier (Bucholc et al., 2011), we monitored changes in fluorescence of AtSCS-B and AtSCS-A (as a control) accompanying binding of calcium. The proteins were excited at 280 nm (monitoring the fluorescence of all fluorophores) or at 295 nm

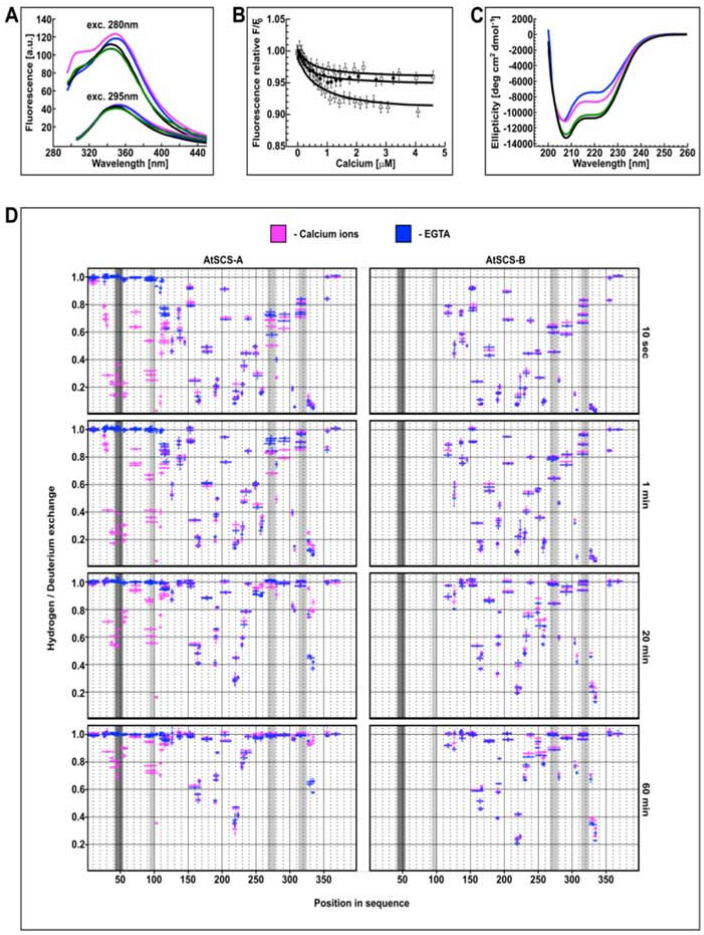

Figure 5.

AtSCS-B Binds Ca^{2+} Without a Substantial Effect on the Protein Conformation. The fluorescence spectra of AtSCS-B and AtSCS-A proteins (A). The fluorescence spectra of 1.2 μM solution of AtSCS-A or AtSCS-B protein, excited at 280 nm (upper curves) or at 295 nm (bottom curves). apo AtSCS-A protein (blue line), apo AtSCS-B protein (black line), holo AtSCS-A (magenta line), and holo AtSCS-B (green line) are presented. The fluorescence spectra represent one of three independent measurements.

The fluorescence titration curves of AtSCS-B protein by calcium ions (B). The fluorescence excitation and the emission were at 280 and 342 nm (open triangles) or 280 and 340 nm (black circles, open squares), respectively. The calcium ions titration of 1.5 μM solutions of AtSCS-B as well as the experimental errors and the theoretical curves, calculated for a single-site ligand binding model (solid lines), are shown.

Conformational changes of AtSCS-A and AtSCS-B proteins upon Ca^{2+} binding. (C) CD spectra of 2 μM solutions of AtSCS-B or AtSCS-A with 1 mM Ca^{2+} (green and magenta lines, respectively) or without Ca^{2+} (100 μM EDTA; blue for apo AtSCS-A and black for apo-AtSCS-B).

Changes of conformational dynamics of AtSCS-A and AtSCS-B upon Ca^{2+} binding. (D) H/D exchange in AtSCS-A (left panels) and AtSCS-B (right panels) in the presence (magenta) or in the absence of Ca^{2+} (EGTA, blue). The proteins were incubated in D_2O buffer for various times (10 sec, 1 min, 20 min, 60 min) and the extent of H/D exchange was determined by mass spectrometry. The horizontal red and blue bars indicate individual peptides identified by mass spectrometry. The X-axis indicates their position in the amino acid sequence of the AtSCS-A. The Y-axis shows relative deuterium uptake calculated as described in Material and Methods; the value 1 represents maximal deuteration level, meaning that all hydrogens in amide bonds of particular peptide were exchanged to deuterium. Error bars are standard deviations from at least three independent experiments. Dark grey – position of calcium binding loops of the canonical EF-hand motif, light grey – positions calcium binding loops of potential non-canonical EF-hand motifs.

344 (monitoring the fluorescence of a Trp residue). AtSCS-B protein has three

fluorophores: Trp72, Tyr29 and Tyr168 (corresponding to Trp182, Tyr139 and Tyr278 in AtSCS-A). The protein fluorescence spectrum is dominated by the broad tryptophan fluorescence band, and the tyrosine fluorescence band is apparent as well. The binding of calcium caused small changes: the small intensity decrease and very small 'red shift' of the maximum, λmax (apo) = 342.5 nm → λmax (*holo*) = 343 nm (for the fluorescence excitation at 280 nm) and λmax (*apo*) = 350 nm → λmax (*holo*) = 351nm (excitation at 295 nm) (Fig. 5A). Also, the small increase of the intensity was observed for the fluorescence band of the tyrosine residue(s), near 305 nm. The fluorescence spectrum of AtSCS-B suggests that the tryptophan residue is buried and inaccessible to an energy transfer from the tyrosine residue(s), and located in an environment that quenches its fluorescence strongly. The calcium binding entails a subtle rearrangement of Trp72 environment, linked with the small red shift of Trp72 fluorescence (at 295 nm excitation) (Fig. 5A).

In parallel, analogous experiments were performed for AtSCS-A protein, as was also studied previously (Bucholc et al., 2011). AtSCS-A protein is longer than AtSCS-B by 110 amino acid residues and richer by one tyrosine residue, Tyr80. The protein is also more sensitive to calcium ions due to the presence of the canonical EF-hand motif. The fluorescence spectra of the AtSCS-A, for *apo* form of the protein, are similar to those of AtSCS-B (Fig. 5A). The most significant fluorescence changes after calcium binding were observed as an increase in the intensity of the tyrosine fluorescence band (Fig. 5A). The contribution of tryptophan residue to those changes is small. The fluorescence spectra excited at 295 nm, are almost the same for the calcium-free and the calcium-bound protein (Fig. 5A, bottom curves), supporting the conclusion that the conformation of the protein in the environment residues Trp182 is only slightly altered by calcium ions. In contrast, the conformation of the protein in the environment of the one or more of the tyrosine residues changes dramatically. Tyr80 present in the N-terminal fragment of AtSCS-A (absent in AtSCS-B protein) seems responsible for these changes. Its fluorescence is influenced most probably by the rearrangement of the canonical EF-hand motif upon calcium binding.

The affinity for calcium of AtSCS-B protein was determined from the fluorescence titration experiments (Fig. 5B). The fluorescence, excited at 280 nm, was measured at 340 or 342 nm, in the fluorescence maximum. The maximal fluorescence intensity changes were small; they did not exceed 10% of the initial fluorescence of the protein (Fig. 5B). To the resulting titration curve, the function describing the binding of

calcium ion [eq. (c), from "Experimental Procedures"] was fitted. The function is analogous with eq. 8 in Eftink (1997) describing single-site ligand binding. The calcium association constant K1 was estimated as $2.4(\pm1.0)\times10^3$ M^{-1}, as the average of three independent measurements. The value of $K1=2.4\times10^3$ M^{-1}, corresponds to a dissociation constant of 0.4 mM.

The stoichiometry of the binding of calcium ions to AtSCS-B was determined from the fluorescence titration curves (Supplemental Fig. S4). The index n equal 1 was estimated based on the Hill equation describing the association of the ligand to the protein, used for the analysis of fluorescence measurements. The resulting formula, derived from the classic Hill equation, is as follows:

$$n = (\log(x/(1-x)) - \log Ka)/\log Lt$$

$$(x/(1-x)) = (F'-1)/(fB-F')$$

where: x – mole fraction of the complex protein-ligand, F' - relative observed fluorescence (relative to the initial fluorescence without the ligand), fB - relative fluorescence of the complex protein-ligand, Lt - the total (free and bound) concentration of ligand, and Ka is the overall association constant of protein-ligand. This result indicates that AtSCS-B molecule most probably binds one calcium ion.

Structural changes of AtSCS-B upon calcium binding were analyzed by far-UV circular dichroism spectroscopy (CD). The binding of calcium ions by the AtSCS-B protein was accompanied by minor structural changes, seen as a decrease of negative CD signals (Fig. 5C) indicating very mild disruption of the protein structure in response to calcium binding, limited to some reduction of helix content or some helix reorientation. In parallel, as a control, the CD spectrum of AtSCS-A protein in the same conditions was analyzed (Fig. 5C). The values of residual molar ellipticity agreed well with the earlier data (Bucholc et al., 2011). The Ca^{2+}-free AtSCS-A protein is 28% helical, and the contribution of helical structures in the Ca^{2+}-bound protein is higher, but less than in AtSCS-B protein (both calcium-free and calcium-bound).

Differences in Conformational Dynamics Between AtSCS-A and AtSCS-B upon Calcium Binding

The analysis of AtSCS proteins using fluorescence and CD spectroscopy methods revealed that the structure of AtSCS-A, but not AtSCS-B, undergoes

significant change upon Ca^{2+} addition; they do not, however, indicate where the conformational changes occur. Therefore, in order to investigate the structure and conformational dynamics of AtSCS proteins in the absence and in presence of Ca^{2+} ions, hydrogen deuterium exchange monitored by mass spectrometry (HDX-MS) was applied. HDX-MS is an analytical technique that maps protein conformational dynamics in solution to specific regions of the protein. The approach applied in this study gave structural information with peptide resolution since the measured degree of exchange is an average over the lengths of the peptides resulting from pepsin digestion. This is especially informative, as to our knowledge no structure of AtSCS-A or AtSCS-B (or any similar proteins) has been determined by X-ray crystallography, Cryo-EM or NMR; none has been deposited in the PDB database.

The hydrogen deuterium exchange patterns along the AtSCS-A and AtSCS-B proteins were obtained for two conditions, one in the presence and in the absence of Ca^{2+} (in buffer with EGTA). Regions could be classified variously as stable or labile, and the stability of some of these regions was calcium dependent, as we describe next.

Conformational dynamics of AtSCS-A - The HDX-MS data show that AtSCS-A protein contains several regions of retarded exchange, independent of the presence of Ca^{2+} (Fig. 5D and Supplemental Fig. S5-S7). Peptides spanning 151-169, 187-196, 215-226 residues can be classified as the most protected (i.e., most stable) regions. These are thus regions involved in the hydrogen-bonding network that constitute the structural core of the molecule. There are also regions along the AtSCS-A sequence for which the level of HD exchange is very high, also independent of the presence of Ca^{2+} ions. Peptides spanning positions 1-19, 110-123, 133-140, 147-160, 197-214, 233-244, 307-325, 351-375 can be classified as the most labile regions. Highly dynamic regions in the inner parts of the SCS protein sequence are probably located within loops and extended turns which connect adjacent elements of the protein.

Some segments of AtSCS-A showed drastically different conformational dynamics depending on the presence of calcium ions. In the presence of EGTA (and absence of calcium), an N-terminal segment of AtSCS-A (region approximately from 20 to 110 amino acid) undergoes very fast HD exchange. This region exhibits no protection even at the lowest measured experimental time of 10 seconds labeling

(Fig. 5D, Supplemental Fig. S5-S7), indicating a lack of secondary structure of this domain. The presence of Ca^{2+} ions dramatically changes the pattern of HD exchange in this region, strongly decreasing the uptake of deuterium in two segments. One of them spans the calcium-binding loop of classical EF-hand motif (fragment 42-53). Unexpectedly, significant changes in the deuterium uptake after Ca^{2+} addition occur also in the region of residues 85-112 (Fig. 5D, Supplemental Fig. S5-S7). In that part of the AtSCS-A, a Prosite motif search algorithm predicted the occurrence of the putative non-canonical EF-hand motif.

Some changes in levels of HD exchange upon Ca^{2+} binding also appear in the AtSCS-A segments 254--301 and 325-337 (Fig. 5D, Supplemental Fig. S6-S7). Two hypothetical EF-hand-like loops (positions: 267-278 and 313-324) are predicted within and close to these fragments. Here, several regions characterized by relatively stable structure were detected. Notably, the retarded exchange is observed in segments directly flanking the putative calcium binding motifs, indicating the presence of stable secondary structure elements there (positions: 245-263 and 325-337). The flanking regions seem to be structured both in the presence and in the absence of calcium ions, whereas the putative EF-hand-like calcium-binding loops exhibit quite high HD exchange levels independent of calcium ions (Fig. 5D and Supplemental Fig. S5 and S6) and can be classified as dynamic regions. Interestingly, the flexibility of fragment 262-301 is decreased when calcium is present (Fig. 5D, Supplemental Fig. S5 and S6). The opposite effect, i.e., destabilization in the presence of calcium, was observed for the region 325-337.

The structure of the common region is more stable in AtSCS-B than in AtSCS-A, both in the presence and in the absence of calcium ions - Patterns of HD exchange obtained in the same experimental conditions for AtSCS-A and AtSCS-B indicate that in general both forms do not differ much from each other in the region 110-250, which is common for both forms (Fig. 5D and Supplemental Fig. S5 and S7). There are however some differences, mainly near putative calcium binding loops (region 157-168 in AtSCS-B, corresponding to 267-278 in AtSCS-A, and 203-214 in AtSCS-B, corresponding to 313-324 in AtSCS-A. Strikingly, in the longer variant (AtSCS-A), regions flanking the predicted calcium-binding loops reveal lower stability than in the shorter variant, which lacks residues 1-110 (AtSCS-B). Thus, the native stability of the C-terminal fragment is disturbed in the structural context of the longer

481 variant. This strongly indicates that the N-terminal domain, absent in AtSCS-B, is
482 structurally coupled to the C-terminal part in AtSCS-A and destabilizes its structure.
483 On the other hand, the HDX data show that in the presence of calcium the third
484 predicted EF-hand-like calcium-binding loop (region 267-278) in AtSCS-A is
485 stabilized in the presence of calcium and becomes similar to that of AtSCS-B. (Fig.5D
486 and Supplemental Fig. S5 and S6)
487
488 **Models of AtSCS-A / AtSCS-B Structure**
489
490 Due to the lack of relevant templates in the PDB, the 3D structure of AtSCS-A
491 was modeled separately for two regions, defined by residue ranges of 1-175 and
492 211-330, respectively. For these protein fragments homology modeling was carried
493 out based on the rationally selected subsets of PDB structures; as described in
494 Methods section.
495
496 **N-terminal domain of AtSCS-A** - The best models for the fragment covering
497 residues 1-175 were built using either 4MBE or 1SL8 PDB records as templates.
498 However, in the hybrid model, obtained by the combination of fragments of 4MBE,
499 4OR9, 1SL8 and 4N5X, modeled structures were scored even better. Since the N-
500 terminal fragment 1-26 was strongly divergent in all models, and was also found
501 flexible in HDX experiments, the subsequent round of modeling was restricted to
502 residues 26-175. The final hybrid model, based on the combination of structural
503 motifs adopted from 2ZND, 1Y1X, 5B8I, 2TN4, 4OR9, scored higher than any of the
504 single structure-based models. The fold of the modeled N-terminal domain shows two
505 pairs of EF-hand-like motifs, the relative orientation of which visibly varies between
506 individual models. However, in the majority of them, the ^{42}**D**Q**D**E**D**G**K**LSVT**E**^{53} loop
507 (Fig. 6A, magenta tube) adopts the canonical conformation characteristic for the
508 calcium-loaded form of EF-hand, whereby calcium is coordinated by the side-chain
509 carboxyl groups of Asp42, Asp44, Asp46 and Glu53, along with the carbonyl oxygen
510 of Lys48 (magenta in Fig. 6A). It should be however mentioned that, according to the
511 review on conservation of individual residues located at the Ca^{2+} binding loop (Halling
512 et al., 2016) Gln, Glu, Lys, Leu, Val and Thr are rarely identified at positions 2, 4, 7, 8
513 and 11 of calmodulin EF-hand motifs (1.0, 1.1, 5.2, 1.8, 2.0 and 3.0 %, respectively).
514 The sequences of the paired loop (^{88}**T**H**G**S**Q**E**K**VSKT**E**^{99}, blue in Fig. 6A) preclude

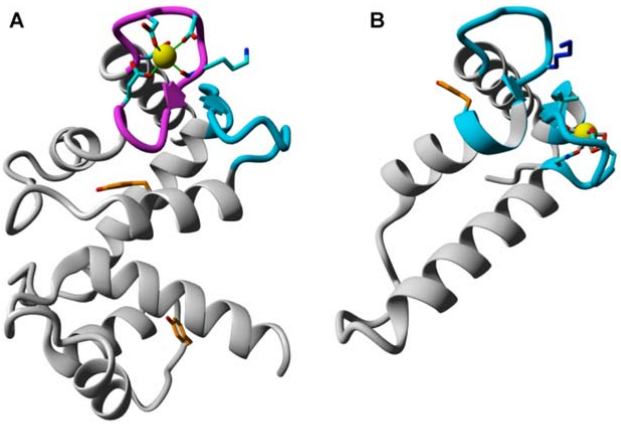

Figure 6.
Modeled by homology structures of N-terminal (residues 26-175) (A) and C-terminal (residues 251-330) (B) parts of AtSCS-A The ribbon representation follows the protein backbone. In magenta and blue are marked peptides predicted as canonical or non-canonical, respectively, EF-hand calcium binding loops. Residues putatively involved in calcium binding are denoted by sticks, yellow spheres represent calcium ions. Tyrosine residues are labeled by orange color.

515 calcium binding. Interestingly, the side chain of Lys94 located in this loop may
516 compete with Ca^{2+} for the binding site, thus stabilizing an EF-hand fold for the *apo*
517 form. Both findings suggest that the N-terminal domain of AtSCS-A binds a single
518 Ca^{2+} cation with an affinity substantially lower than that of calmodulin, which confirms
519 our previous data describing Ca^{2+}-binding properties of AtSCS-A (Bucholc et al.,
520 2011).

521 Finally, it should be mentioned that both tyrosine residues (Tyr80 and Tyr139,
522 orange in Fig. 6A) are buried, and fluorescence of Tyr80 should be affected by
523 calcium binding, what is in agreement with our results of the analysis of AtSCS-A in
524 respect of changes in fluorescence upon binding of calcium.
525
526 **C-terminal domain of AtSCS-A / AtSCS-B** - There were no appropriate
527 templates for the C-terminal fragment (residues 331-378). The best model for the
528 fragment defined by residues 211-330 was based on 1PRW, and no further
529 improvement was achieved for the hybrid models. However, detailed inspection of
530 the alternative highly scored models (e.g., based on 1QTX or 4AQR) clearly shown
531 that only the fragment covering residues 251N-A330 could be reasonably modeled,
532 while the homology-modeled structure of 211-250 critically depends on the template
533 protein used. The subsequently built hybrid model for 251N-A330 was based on
534 3TZ1, with some parts improved using alternative models based on 1QTX, 1RFJ,

3WFN and 1PRW. The resulting structure represents pair of EF-hand-like motifs, one of which (^{313}NG**D**D**G**NVVKEEE^{324}) may display propensities toward binding of calcium via side-chain oxygen atoms of N313, D315 and E324, and backbone carbonyl groups of G317 and V319, the affinity of which must be expected much lower than that for N-terminal part of the protein. This loop is putatively paired with (^{267}PK**D**RQGKVSKGY^{278}), sequence of which preclude any interaction with calcium (Fig. 6B). It should be noted that side chain of K273 might interact with the ^{313}NGDDGNVVKEEE^{324} loop, thus mimicking calcium-loaded EF-hand state.

Our HDX data indicate interplay between the N-terminal part of AtSCS-A (containing the canonical EF-hand motif) and the C-terminal part (containing only EF-hand-like motifs). Both domains seem to be structurally coupled in AtSCS-A, and strong structuring of the N-terminal region of the AtSCS-A upon Ca^{2+} binding affects this interaction. Calcium-induced structuring of the AtSCS-A N-terminal domain may influence the dynamics of distant parts, which are already well structured in the *apo* form (Fig. 5D). It is possible that the small changes observed in the C-terminal fragment of AtSCS-A upon binding of calcium do not indicate direct calcium binding to this domain, but may originate from an allosteric transmission caused by the calcium binding to the canonical site in the N-terminal domain. Fragment 325-337 FKKTMAEILGSIM, whose stability in AtSCS-B is nearly independent of the presence of Ca^{2+}, is definitely less stable in AtSCS-A *apo*, and is even much more destabilized in AtSCS-A in the presence of calcium ions (Fig. 5D, Supplemental Fig. S6 and S7). In contrast, the region 278-283 YLRAVL (Supplemental Fig. S7 and S8) in AtSCS-A in the presence of Ca^{2+} becomes stabilized and at least in 1 min of exchange resembles this fragment within AtSCS-B.

According to the model, the first calcium-binding domain (canonical EF-hand motif) forms a classical helix-turn-helix structure with helices 26-40 and 57-63 (Fig. 6A). This model agrees well with the HDX data. In the presence of Ca^{2+}, regions characterized by the strongest retardation of HD exchange cover the 28-62 fragment (representing canonical EF-hand motif), and additionally the 85-115 one, where the EF-hand-like motif is predicted. The helices of canonical EF-hand and non-canonical EF-hand exhibit similar HD exchange patterns, with a strongly retarded exchange in the presence of Ca^{2+} with the exception of the helix at 77-87, where HD exchange is much faster. The model predicts proximity of the canonical EF-hand motif and the non-canonical one. For canonical EF-hand motif the lowest level of HD exchange is

observed within loop 41-56 constituting Ca^{2+} binding sites, for non-canonical EF-hand the lowest level of HD exchange refers to fragment 101-106 within helix 99-117 (Fig. 5D and Supplemental Fig. S7 and S8).

Modeling of the region 250-330 predicts the existence of four helices (252-256, 275-287, 297-313, 321-326) (Fig. 6B). Indeed, in the HDX experiment there is significant retardation in HD exchange within helix 252-256, 275-287, 297-313 and 321-326 (Fig. 5D and Supplemental Fig. S8). The structural model predicts direct contact between helices. HDX technique confirms the stability of regions above, consistent with the modeled interaction between adjacent helices, which should significantly stabilize the network of hydrogen bonds and create a connected and coherent structure (Fig. 6B).

DISCUSSION

Depending on a variety of environmental cues, plants trigger appropriate responses from among diverse signaling pathways, activating specific defense mechanisms and adjusting plant development to new conditions. SnRK2 kinases play a key role in the regulation of the ABA-dependent development and responses to water deficit, as well as several other stresses. They are known as calcium-independent enzymes; however, several data indicate their interplay with calcium signaling pathways. Calcium-dependent kinases, CIPKs, together with SnRK2.6 phosphorylate and regulate activity of NADPH oxidase (respiratory burst oxidase homolog F, RbohF; Sirichandra et al., 2009 and Han et al., 2019), whereas CDPKs along with SnRK2s activate the guard cell S-type anion channel (SLAC1) in response to ABA (Geiger et al., 2010; Brandt et al., 2012). Importantly, in the *snrk2.2/snrk2.3/snrk2.6* knockout mutant the Ca^{2+}-dependent SLAC1 regulation was impaired (Brandt et al., 2015) indicating interconnection between SnRK2s and calcium signaling pathways. Furthermore, in 2003 Harmon predicted that calcium could somehow regulate SnRK2s (Harmon, 2003); C-terminal parts of SnRK2 kinases are rich in acidic amino acids, and those can be potentially involved in Ca^{2+}-binding. Our previous results showed that indeed Ca^{2+} added to SnRK2s slightly affected their kinase activity (Bucholc et al., 2011). However, a much more significant Ca^{2+}-dependent effect on their activity arises via their cellular inhibitory partner, SCS, a calcium sensor (Bucholc et al., 2011).

Our present results show that in Arabidopsis, due to alternative transcription start sites, two forms of *AtSCS* are expressed, *AtSCS-A* and *AtSCS-B*. They encode proteins that differ only in the N-terminal region; AtSCS-B is thus a shorter version of AtSCS-A in which the first 110 aa are missing. This region includes the classical EF-hand and the first EF-hand-like motifs. The basic properties of AtSCS-A have been previously described by Bucholc et al. (2011). Now, we analyzed biophysical and biochemical features of AtSCS-B, and performed detailed comparative studies of both proteins in respect of their conformational dynamic with and without calcium, inhibition of the SnRK2 activity and their role in the plant response to water deficit.

The data presented here indicate that only AtSCS-A can play a role as a calcium sensor. The calcium-binding constant of this protein as determined previously by the protein fluorescence titration was 2.5 (±0.9) x 10^5 M^{-1},

corresponding to a dissociation constant of 4 μM (Bucholc et al., 2011). The calcium binding induces significant conformational changes of the protein as revealed by CD spectroscopy and HDX-MS analysis, indicating a possible function of AtSCS-A as a calcium sensor in plant cells. *In vitro* studies demonstrate the SnRK2 inhibition occurs only in the presence of calcium. On the other hand our data showed that even though AtSCS-B binds calcium ions, the binding is two orders of magnitude weaker than that for AtSCS-A and there are no conformational consequences of the calcium binding. These data indicate that for the inhibition of the SnRK2 activity is responsible the common region of AtSCS-A and AtSCS-B. The primary structures of both proteins in this region are identical, than the question appears why AtSCS-A requires Ca^{2+} for the inhibition and AtSCS-B does not. The mechanism of the SnRK2 inhibition by SCS is still an open question and needs further study, but the conformational dynamics of both AtSCSs in the presence and absence of calcium ions shed light on calcium dependence on the SnRK2 inhibition in the case of AtSCS-A. Our HDX-MS results provide extensive analysis of the changes of the conformational dynamic of proteins with classical and non-classical EF-hand motifs upon calcium binding and indicate that N-terminal part of AtSCS-A has a great impact on the C-terminal part.

Our results showed clearly that the domain common to both variants, i.e., the C-terminal fragment of AtSCS-A, is much less stable in the longer form than in the shorter form. HDX-MS and CD analysis indicate that in AtSCS-B this region forms stable structures independent of calcium, with no significant increase in stability in the presence of calcium. In AtSCS-A, the N- and C-terminal segments, though distant in sequence, are structurally coupled, so the C-terminal part has properties distinct from those of AtSCS-B. In AtSCS-A the dynamics of the elements of the C-terminal domain become calcium-sensitive, unlike in AtSCS-B, where calcium-induced changes are negligible. Binding of calcium destabilizes region 321-340 in the C-terminal domain while it reverses the destabilization of the loop of the predicted third EF-hand-like motif (267-278) and the flanking region (278-283). In the presence of calcium ions, the conformational dynamics of this fragment becomes similar to that of the same region in AtSCS-B. Based on these data, we predict that the third EF-hand like motif in AtSCS-A and the motif corresponding to this region in AtSCS-B are probably critical for inhibition of the SnRK2 activity. The conformation of this region required for the kinase inhibition is the one which is present in AtSCS-B (independent

of calcium), but which in AtSCS-A requires the presence of calcium. This would explain why AtSCS-A needs calcium ions for the inhibition, whereas AtSCS-B does not.

Moreover, our HDX-MS results show interesting data on the cooperation of Ca^{2+} binding by canonical and non-canonical EF-hand motifs. Upon calcium binding, the region of the predicted calcium-binding loop of the classical EF-hand motif present in AtSCS-A and adjacent regions become much more stable (HDX-MS data), and the overall structure becomes more helical (CD data), Interestingly, according to HDX results, the segment 85-115 (predicted putative EF-hand-like motif with very low identity with the canonical motif) also undergoes significant stabilization in response to Ca^{2+} addition. The changes in deuterium uptake after Ca^{2+} addition in this region were similar to those observed for the canonical motif. It is plausible that the changes observed in the non-canonical motif are not a result of calcium binding in this region, but they are an indirect effect of calcium binding at the canonical site. The vast majority of EF-hand motifs (and almost all fully functional ones) exist in pairs, usually structurally coupled by a short β-sheet (β-scaffold) that maintains a direct contact between metal ion-binding loops (for a review see, Nelson et al., 1998). It is possible that the non-canonical motif cooperates with the canonical motif in calcium ion binding and plays a role of a structural scaffold, influencing the properties of the canonical site. The HDX-MS technique is not able to distinguish between conformational changes resulting from direct ligand binding or allosteric effects triggered by an interaction in a different part of the molecule.

Finally, we analyzed the effect of AtSCS-A and AtSCS-B on plant response to stress using a transgenic approach. We generated transgenic Arabidopsis plants expressing *AtSCS-A-c-myc* or *AtSCS-B-c-myc* in the *scs-1* knockout mutant background. We did not observe any significant differences between the plants of the transgenic lines, the WT plants, and the *scs* knockout mutants grown in optimal conditions. Since SnRK2s are key regulators of the plant response to water deficit (Fujii and Zhu, 2009; Fujita et al., 2009; Nakashima et al., 2009) we analyzed the effect of AtSCS-A and AtSCS-B in the plant response to dehydration. The results showed that both forms of AtSCS are involved in response to this stress; the *scs* mutants were more resistant to dehydration than the WT plants and plants expressing *AtSCS-A-c-myc* or *AtSCS-B-c-myc.* We did not observe significant differences between the transgenic lines expressing one or another form of AtSCS.

The only difference we observed was a less pronounced effect of AtSCS-B than that of AtSCS-A; only in the line B12, in which the expression of AtSCS-B was very high, we observed inhibition of the SnRK2 activity and a meaningful effect on the dehydration response. Importantly, the expression of each of the forms was not able to fully compensate the *scs* mutation, suggesting that both forms are involved in the regulation and their role is not fully overlapping. We obtained similar results using two independent assays, drought tolerance test and water loss in detached rosettes. Based on observed differences in the localization of SnRK2-AtSCS-A and SnRK2-AtSCS-B complexes *in planta* (BiFC assays) we can speculate that both AtSCS forms might regulate phosphorylation of diverse proteins in plant cells. However, it should be noted that the effect of both AtSCSs on the plant response to water withdrawal is similar to but less pronounced than the effects of clade A phosphatases, which are considered as the major negative regulators of the SnRK2s activity.

The analysis of the kinase activity in the transgenic plants showed that both SCSs inhibit the ABA-responsive SnRK2s. Still we cannot exclude that AtSCS-A also inhibits the ABA-non-responsive SnRK2s, since AtSCS-A in contrast to AtSCS-B interacts not only with the ABA-activated SnRK2s but also with kinases of the group 1, which are not activated by ABA. However, the evolution studies performed by Holappa et al. (2017) have shown that SCS proteins appeared in earliest land plants at about the same time as ABA receptors - RCAR/PYR/PYL (RCAR, Regulatory Component of ABA Receptor/PYR1, Pyrabactin Resistance 1/PYL, PYR1-like), PP2Cs (Umezawa et al., 2010; Komatsu et al., 2013; Shinozawa et al, 2019), and ABA-activated SnRK2s (from group 3) that constitute the prototype of the SnRK2 family. The ABA-non-responsive SnRK2s evolved later, in vascular plants. Thus, the ABA-activated SnRK2s, RCAR/PYR/PYLs, PP2Cs, and SCSs seem to consist of ancient regulatory modules of ABA signaling, allowing adaptation to a terrestrial environment.

CONCLUSIONS

Our studies showed that two isoforms of ASCSs (AtSCS-A and AtSCS-B) are expressed in Arabidopsis. They differ significantly in their expression profiles, calcium

binding properties, and conformational dynamics. Both of them inhibit the activity of the ABA-activated SnRK2s and regulate the plant response to water deficit similar to the clade A PP2C phosphatases, although the effect of AtSCSs is not as strong as the one observed in the case of the phosphatases. Moreover, the results provide information on calcium binding properties and conformational dynamics of EF-hand and EF-hand-like motifs present in plant proteins. This extends our knowledge on proteins involved in fine-tuning of the SnRK2 activity in stress signaling in plants, connecting calcium-independent and calcium-dependent pathways.

MATERIALS AND METHODS

Plant Materials, Growth Conditions, and Stress Treatments

Arabidopsis thaliana lines used in this study include: Col-0 as the wild type background, T-DNA insertion lines; *scs-1* (Salk_051356) and *scs-2* (Salk_104688) previously described (Bucholc et al., 2011), *snrk2.6* (Salk_008068) obtained from the Nottingham Arabidopsis Stock Center, double mutant *snrk2.2/2.3* (GABI-Kat 807G04/Salk_107315) provided by Jian-Kang Zhu, (Purdue University), a quadruple knockout mutant *snrk2.1/2.4/2.5/2.10* (SAIL_*519_C01*/Salk_*080588*/Salk_*075624*/WiscDsLox233E9) described by Maszkowska et. al., 2018 and double mutant *abi1-2/pp2ca-1* (Salk_72009/Salk_28132) obtained from Pedro L. Rodriguez (Instituto de Biologia Molecular y Celular de Plantas). The seeds of *Arabidopsis thaliana* were grown under long day conditions (16-h-light/8-h-dark photoperiod) at 22°C/18°C in soil or in hydroponic culture (Araponics System) as described by Kulik et al., 2012. For expression analysis of *AtSCS-A* and *AtSCS-B* in response to ABA or salt, plants were grown at 21°C/21°C under mid-day conditions (12-h-light/12-h-dark cycle) for 2 weeks in hydroponic culture and seedlings were either mock treated or with 10 µM ABA or 150 mM NaCl, respectively, at specific times. After treatment plants were collected, frozen in liquid nitrogen and stored at -80ºC until analyzed. For aseptic cultures, seeds were sterilized in 70% ethanol for 2 minutes then in a water/bleach solution 13:1 (v/v) for 20 minutes. After sterilization, the seeds were extensively washed with sterile water. Seeds were stratified in the dark at 4°C for 3 days. For

752 transient expression experiments, protoplasts were isolated from *Arabidopsis*
753 *thaliana* T87 cells grown in Gamborg B5 medium as described by (Yamada et al.,
754 2004), six days after subculturing.
755
756 **_AtSCS-A_ and _AtSCS-B_ Expression Analysis in Arabidopsis**
757
758 AtSCS-A and AtSCS-B expression was analyzed by two-step RT-qPCR. Total
759 RNA was extracted from Arabidopsis seedlings or different organs using a Thermo
760 Scientific GeneJet Plant RNA Purification Mini Kit and treated with Thermo Scientific
761 RapidOut DNA Removal Kit. The efficiency of DNA removal was monitored by PCR
762 with primers for PP2A. First-strand cDNA synthesis was performed using 1.5 µg of
763 total RNA with oligo $(dT)_{18}$ primer and Thermo Scientific RevertAid First Strand cDNA
764 Synthesis Kit according to standard manufacturer's protocol. Relative expression
765 levels were determined by quantitative PCR in a LightCycler® 480 Roche device,
766 using SYBR GREEN mix (Roche). For each target gene amplification, two gene-
767 specific primers were used (listed in Supplemental Table S1) and all cDNA samples
768 (three replicates) and standards (two replicates) were assayed in a single run.
769 Relative gene expression in each sample was calculated using standard curve
770 method (5-point), normalized using a geometric mean of expression values for two
771 reference genes (*PDF2* and *UBC21*) and scaled to the calibrator sample (Col-0
772 control).
773
774 **Expression of Recombinant Proteins**
775
776 Expression of recombinant proteins in *Escherichia coli* was performed as
777 previously described (Bucholc et al., 2011). cDNA encoding AtSCS-B or fragment of
778 ABF2 (Gly73 to Gln120) was PCR amplified using appropriate primers (listed in
779 Supplemental Data) and cloned into pGEX-4T-1 vector (GE Healthcare Life
780 Sciences). The PCR reaction was performed using a high-fidelity Pfu DNA
781 polymerase (Stratagene, La Jolla, CA) and verified by sequencing.
782
783 **Purification of Recombinant Proteins**
784

All recombinant proteins were purified using glutathione-sepharose beads (GE Healthcare Life Sciences) as previously described by Bucholc et al., 2011. To obtain highly purified AtSCS-A and AtSCS-B proteins the last step of purification was reverse-phase HPLC on an analytical ACT Ace C18 column (for analysis of calcium binding) or Mono Q column using an FPLC system (GE Healthcare Life Sciences). Purity of the proteins was analyzed by SDS-PAGE and electrospray ionization mass spectrometry on a Micromass Q-TOF spectrometer (Micromass, Manchester, Great Britain). GST-ABF2$^{73\text{-}120}$ fusion protein after purification using glutathione-sepharose beads (GE Healthcare Life Sciences) was precipitated with chloroform/methanol and resolubized in 10mM Tris-HCL, pH8.8, 0.1% SDS.

Protein Kinase Activity Assays

The kinase activity assay in solution was performed as described by Bucholc et al., 2011.

In-gel kinase activity assays were performed according to Wang and Zhu, 2016 with some modifications. Proteins were extracted from 14-d-old seedlings grown in hydroponic culture in flasks that were either mock-treated or with 100µM ABA, 350 mM NaCl for 0, 30, 60 min. Plant materials from wild-type (Col-0) and different mutant lines were ground in liquid nitrogen and sonicated three times in the buffer (50 mM HEPES-KOH, pH 7.5, 5 mM EDTA, 5 mM EGTA, 2 mM DTT, 25 mM NaF, 1mM Na_3VO_4, 50 mM ß-glycerophosphate, 10% (v/v) glycerol, 1mM PMSF, 1x protease inhibitor cocktail (Roche) and 1x phosphostop (Roche). Proteins (40 µg/lane) in Laemmli buffer (without boiling) were separated on a 10% SDS-PAGE containing 0.25 mg/mL GST-ABF2$^{Gly73\text{-}Gln120}$ or 0.5 mg/mL myelin basic protein (MBP) (Sigma-Aldrich) as a kinase substrate. The gels were run over-night at 30 V and next washed for 3 x 30 min at room temperature (RT) in SDS removal buffer (25 mM Tris-HCl, pH 7.5, 0.5 mM DTT, 5 mM NaF, 0.1 mM Na_3VO_4, 0.5 mg/mL BSA, 0.1 % Triton X-100). After that, the gels were incubated in renaturing buffer (25 mM Tris-HCl, pH 7.5, 1mM DTT, 5 mM NaF, 0.1 mM Na_3VO_4) for 2 x 30 min at RT, over-night at 4°C and 1 x 30 min at RT. After 30 min of incubation at RT in cold kinase reaction buffer (25 mM Tris-HCl, pH 7.5, 1 mM EGTA, 30 mM $MgCl_2$, 2 mM DTT, 0.1 mM Na_3VO_4,) the gels were incubated in 10 ml of hot kinase reaction buffer supplemented with 50µCi of [γ-^{32}P] ATP for 5 min at RT and after addition of 20µM of cold ATP for 90

819 min at RT. The reaction was stopped with stop washing solution (5% TCA and 1%
820 sodium pyrophosphate). After extensive washing with washing buffer the gels were
821 stained with Coomassie Brilliant Blue R250, dried and exposed to autoradiography.
822
823
824 **Yeast Two Hybrid and Bimolecular Fluorescence Complementation (BiFC)**
825 **Assays**
826
827 Yeast two-hybrid analysis was carried out as described previously by Bucholc
828 et al., 2011. The cDNAs encoding SnRK2s were cloned into pGBT9 vector (Clontech)
829 and *AtSCS-A* or *AtSCS-B* were cloned into pGAD424 (Clontech). Primers used for
830 cloning are listed in Supplemental Table S1.
831 For subcellular localization analysis coding sequences for AtSCS-A and
832 AtSCS-B were introduced into pSAT6-EGFP-N1 or pSAT6-EGFP-C1. For BiFC
833 assays, constructs for *SnRK2s* expression were prepared in pSAT4-nEYFP-C1 and
834 *AtSCS-A* or *AtSCS-B* in pSAT1-cEYFP-N1 or pSAT1-nEYFP-N1, respectively. The
835 pSAT vectors were provided by Prof. T. Tzfira (Tzfira et al., 2005). Primers are listed
836 in Supplemental Table S1. Subcellular localization and BiFC analyses were
837 performed as described by Bucholc et al., 2011. Subcellular localization of the EGFP
838 fusion proteins and EYFP fluorescence after complementation were evaluated using
839 a Nikon C1 confocal system built on TE2000E inverted microscope and equipped
840 with a 60×/1.4 NA Plan-Apochromat oil immersion objective (Nikon Instruments B.V.
841 Europe, Amsterdam, Netherlands). EGFP and EYFP were excited with a Sapphire
842 488 nm laser (Coherent, Santa Clara, CA, USA) and observed using the 515/530
843 emission filter. For publication, single optical sections with distinctly visible nucleus
844 and nucleoli were selected to ensure that similar focal planes were compared for all
845 tested variants. Images were processed using Nikon EZ-C1 Free Viewer (version
846 3.90).
847
848 **Calcium Ion Binding Analysis**
849
850 For calcium binding analysis, the recombinant proteins were purified by
851 reverse-phase HPLC on an analytical ACT Ace C18 column; their purity was
852 estimated by electrospray ionization mass spectrometry. Protein concentration was

determined from UV absorption at 280 nm, using the molar extinction coefficients of 10500 M^{-1} cm^{-1} and 9300 M^{-1} cm^{-1} for AtSCS-A and AtSCS-B, respectively, as calculated for one Trp and three Tyr residues (AtSCS-A) or one Trp and two Tyr residues (AtSCS-B) (Mach et al., 1992). The UV absorption spectra were measured on a Cary 3E spectrophotometer (Varian) in thermostated cells of 10 mm path length. 20 mM Tris buffer, pH 7.4, with 100 mM NaCl was used as a solvent for the calcium binding experiments. All measurements were performed at 20°C.

Fluorescence Measurements - The protein fluorescence was measured on a CaryEclipse fluorimeter. Spectra were collected with an average time of 2 s for each point and a step size of 0.5 nm from 295 (or 305) to 450 nm. In fluorescence titration experiments small aliquots of concentrated calcium chloride solution were added until the protein fluorescence no longer changed. The measurements were repeated at least three times. All protein solutions used in the fluorescence titration experiments were checked for possible calcium contamination by comparing the protein fluorescence signals in the presence and absence of calcium chelator (100 μM EGTA).

Calcium Ion Binding Constant - The measured fluorescence signal (F) is defined as:

$$F = F0 \times xF + F1 \times x1 \qquad (a)$$

where F0, F1, are fluorescence of the protein without and with the ligand, respectively. The xF and x1, are mole fractions of free protein (PF, no ligand bound) relative to total protein (P0), xF=PF/P0, and ligand bound protein (P1), x1=P1/P0, respectively. The two mole fractions sum to one: xF +x1 =1.

The binding constant of the ligand to the protein in a reaction, $P + L \rightleftarrows PL$ is defined as:

$$K1 = P1/(PF \times LF) \qquad (b)$$

where, P0=P1+PF and L0=LF+P1 are total concentrations of the protein and the ligand, respectively. If F'= F/F0 and f1 = F1/F0, then:

$$F' = 1-x1 + f1 \times x1 \qquad (c)$$

The equation is analogous with that of eq. 8 in (Eftink, 1997) describing single-site ligand binding, where the variables are F' (from experimental measurements), total ligand concentration, L0, and protein concentration, P0, and the parameters are the ligand binding constant, K1, and relative fluorescence signal, f1. Here, the ligand is

886 Ca^{2+} ion. The parameter values were determined by least-square fitting of theoretical
887 curves to experimental data using the NiceFit program.
888
889 **Circular Dichroism Measurements**
890
891 Circular dichroism (CD) experiments were carried out at 20°C on Jasco J-815
892 spectropolarimeter with a 10 mm path length cuvette. The protein solutions (close to
893 2 μM) were prepared in 5 mM Tris buffer, pH 7.4, with 100 mM NaCl. CD spectra
894 were collected twice with an average time of 2 s for each point and a step size of 1
895 nm from 200 to 270 nm. All spectra were corrected against the buffer. The data were
896 converted to molar residue ellipticity using the relationship $[\Theta]= \theta/(10\times n\times l\times c)$, where
897 $[\Theta]$ is molar residue ellipticity in (degree cm^2 $dmol^{-1}$), θ is the observed ellipticity in
898 millidegrees, n is the number of aminoacid residues in the protein, l is the path length
899 in cm, and c the protein concentration in M.
900 The secondary structure content of the proteins was estimated using the
901 CDNN program (CD spectroscopy deconvolution software) (Böhm et al., 1992).
902
903 **Hydrogen Deuterium Exchange Coupled to Mass Spectrometry**
904
905 The HDX-MS was performed as described previously (Sitkiewicz et al., 2013),
906 with minor modifications. Initially, the list of peptides was established by diluting each
907 analyzed protein to 5-10 μM in a non-deuterated buffer (50 mM Tris pH 7.4, 150 mM
908 NaCl). Each sample (50 μL) was acidified by adding 10 μL of "stop" buffer (2M
909 glycine pH 2.5, 150mM NaCl, 4M GuHCl) and then injected into a Waters
910 nanoACQUITY UPLC system equipped with an HDX Manager system (Waters) with
911 the column outlet coupled directly with SYNAPT G2 HDMS mass spectrometer.
912 Rapid online digestion on an immobilized pepsin column (Poroszyme, ABI) was
913 performed at a flow 200 μL/min. Peptides were captured on a trapping BEH C18 1.7-
914 mm, 2.1×5mm Vanguard Pre-Column (Waters) and separated by 1.0×100 mm BEH
915 C18 1.7-mm analytical reversed phase column (Waters) with a gradient of 8-40 %
916 acetonitrile (0.1 % formic acid) in 6 minutes at a flow 40 μL/min. All capillaries,
917 valves, and columns were maintained at 0.5°C inside a HDX cooling chamber, while
918 the pepsin column was kept at 13°C inside the temperature-controlled digestion
919 compartment. Mass spectra were acquired in MSE mode over the m/z range of 50-

2000 both with and without ion mobility separation. Spectrometer ion source parameters were as follows: ESI positive mode, capillary voltage 3 kV, sampling cone voltage 35 V, extraction cone voltage 3 V, source temperature 80°C, desolvation temperature 175°C, and desolvation gas flow 800 L/h. Infusion and scanning every 30 seconds of leu-enkephalin (556.277 m/z) was used for continuous lock mass correction. Rigorous washing steps were performed between each injection. The peptides were identified with ProteinLynx Global Server software (Waters) using randomized database and with false discovery rate threshold set to below 4%.

Deuterium labeling was initiated with a 10-fold dilution of the protein sample into a buffer containing 50 mM Tris, pH 7 (uncorrected meter reading), 150 mM NaCl and 5 mM $CaCl_2$ or 5 mM EGTA in 99.8% D_2O (Cambridge Isotope Laboratories, Inc.). After a specified time (10 s, 1 min, 20 min, 60 min) the labeling reaction was quenched by adding “stop” buffer and then the sample was immediately snap-frozen in liquid nitrogen and stored at −80°C until analyzed. Quenched samples were rapidly thawed and injected into a Waters nanoACQUITY LC system equipped with HDX Manager, coupled directly with SYNAPT G2 HDMS mass spectrometer. “Out” controls of back exchange level were performed by incubation of the protein in D_2O buffer for 48 hours to obtain maximum exchange for each peptide. The experimental maximum is always lower than the maximal theoretical exchange due to a certain degree of back exchange. Each experiment was repeated at least three times and the results represent the mean of all replicates.

Data analysis. Peptide list for each protein was created in the DynamX 3.0 software based on PLGS peptide identifications, with following acceptance criteria: minimum intensity threshold - 5000, minimum fragmentation products per amino acids for precursor - 0.3, the maximum mass difference between the measured and theoretical value for parent ions - 10 ppm. Analysis of the isotopic envelopes in DynamX 3.0 software was carried out using the following parameters: retention time deviation ± 18 s, m/z deviation ± 15 ppm, drift time deviation ± 2 time bins and centroids of the mass envelopes were obtained. The values reflecting the experimental mass of each peptide in all possible states, replicates, time points and charge states were exported from the DynamX 3.0 and further data analysis was carried out using in house scripts written in R language (http://www.R-project.org). Fraction exchanged (D) was calculated with the following formula:

$$D=((M\_ex–M\_ex\ 0))/((M\_ex\ 100–M\_ex\ 0))$$

where: (Mex0) and (Mex100) indicate the average peptide mass measured in the unlabeled sample and mass from "out" control, respectively. Error bars for fraction exchanged represent standard deviations calculated from at least three independent experiments. The difference in the fraction exchanged (Δ fraction exchanged) was calculated by subtracting the fraction-exchanged values for peptides in the selected state from the values for the same peptides in the control state. The error bars were calculated as the square root of the sum of the variances from compared states. Student's t-test for two independent samples with unequal variances and unequal sample sizes (also known as Welsh t-test) was carried out to evaluate differences in fraction exchanged between the same peptides in two different states.

Construction and selection of transgenic Arabidopsis thaliana plants

To generate the transgenic lines in *scs-1* background coding sequences for AtSCS-A and AtSCS-B were cloned into pENTR-®-D/TOPO™ vector (Thermo Fisher) and next, the cDNAs were recombined by Gateway LR reaction into pGWB617 destination vector (Nakamura et al.,2010). The pGWB617-AtSCS-A and pGWB617-AtSCS-B constructs were transformed via *Agrobacterium tumefaciens* strain GV3101 into mutant background *scs-11* by the floral dip method as previously described by Clough & Bent, 1998 and Zhang at al., 2006. The selection of the transgenic lines was performed by spraying soil-grown seedlings with 0.033% BASTA solution supplemented with 0.01% Silwet L-77 at 7 and 9-day after germination. Recombinant proteins were confirmed by western blot analysis using a c-Myc monoclonal antibody (9E10, Santa Cruz) according to the protocol recommended by the manufacturer.

Rosette water loss measurement

The Arabidopsis plants of the appropriate genotype were grown for ~~5~~–6 weeks under short day conditions (8 h light at 22°C / 16 h dark at 20°C) in a CLF PlantClimatics chamber incubator and watered copiously one day before harvest. The Cut Rosette Water Loss (CRWL) was determined as described previously by Bouchabke et al. (2008) with minor modifications. Freshly cut rosettes were weighed immediately, incubated in windless conditions under constant temperature (22-24°C) and weighed

five times hourly. After overnight drying at 70°C to a constant mass, the rosettes were weighed for dry mass, and water loss was calculated.

Drought tolerance test

The Arabidopsis plants were grown in pots (approximately 50 plants per pot) for 17 days under long-day conditions (16 h light at 22°C / 8 h dark at 20°C) and for an additional 2 weeks without watering. After that time, the plants were watered. Pictures were taken before re-watering and on the second day of re-watering.

Modeling of AtSCS-A/B Structure

Since no structures of AtSCS variants have been available in the PDB, they were modeled by homology using algorithms implemented in Yasara (Krieger et al., 2002; Krieger et al., 2009). In every round of modeling 12 protein structures sequentially close to the target were used as initial templates. For each template up to 5 alternative alignments with the target sequence were used, and up to 50 different conformations were tested for each loop being modified. The resulting models were individually scored according to their structural quality (dihedral distribution, backbone and side-chain packing), and those with the highest scores were further used to form a hybrid model, which was built using the best fragments (e.g. loops) identified among the single-template models. However, due to limited coverage with sequences of proteins with known structure, AtSCS-A has to be modeled as the two separate domains, relative orientation of which remains unknown. In accordance with HDX-MS data, the N-terminal one covered residues 26-175, while the C-terminal corresponded to residues 211-330.

ACKNOWLEDGMENTS

We thank dr. Olga Sztatelman (IBB PAN, Warsaw, Poland) for providing pGBT9-SnRK2.3, pGBT9-SnRK2.7, pGBT9-SnRK2.9 plasmids and *snrk2.1/4/5/10* knockout mutant. We are also grateful to Professor Zhu-J-K and Pedro I. Rodriguez for sharing with us the *snrk2.2/2.3* and *abi1-2pp2ca-1* knockout mutants, respectively, and all

members of our laboratory for stimulating discussions. We also thank Nottingham Arabidopsis Stock Center for providing the *snrk2.6* mutant.

FIGURE LEGENDS

Figure 1.

The expression of AtSCS-A and AtSCS-B varies across plant organs and in plant response to ABA or NaCl treatment. Alternative isoforms of AtSCS (At4g38810), AtSCS-A and AtSCS-B, predicted at transcript (A) and protein (B) levels. The prediction was done based on TAIR plant promoter database (PlantPromoterDB) and Prosite (prediction of EF-hand motifs).

Quantitative RT-PCR analysis of *AtSCS-A* and *AtSCS-B* transcript levels in different organs (C) in seeds during germination (D), in 2-week-old seedlings exposed to 10 µM ABA (E) or 150 mM NaCl (F). Figures E and F - expression levels in plants exposed to ABA or NaCl (dark grey), whereas in control plants, mock treatment (light grey). Data represent means of triplicate biological repeats, and the error bars indicate SD. For statistical analysis a two-tailed *t*-test in Microsoft Office Excel was applied. The asterisks indicate significant difference from the wild type (*P < 0.05; **P < 0.01, ***P < 0.001).

Figure 2.

AtSCS-B interacts preferentially with kinases that belong to group 2 and 3 of the SnRK2 family. Interactions between Arabidopsis SnRK2s and AtSCS-B, or AtSCS-A as a control, were analyzed by a yeast two-hybrid assay (A), as described in Bucholc et al., 2011. Yeast transformed with a construct with cDNA encoding one of the analyzed SnRK2 and complementary empty vector (BD-SnRK2+AD), or a construct with AtSCS-B or AtSCS-A and the other empty vector (BD+AD-AtSCS) were used as controls. The growth of yeast expressing the indicated constructs was monitored on selective media: without Leu and Trp (-LW); without Leu, Trp and His and with 8mM AT (-LWH); without Leu, Trp and Ade (–LWA). AD, Gal4 activation domain; BD, Gal4 binding domain.

The subcellular localization of AtSCS-B was analyzed in Arabidopsis protoplasts (B), as described in Bucholc et al., 2011. Protoplasts isolated from the T87 Arabidopsis

cell line were transiently transformed with plasmid encoding AtSCS-B-EGFP and its localization was analyzed by confocal microscopy.

Interaction between AtSCS-B and SnRK2s *in planta* was analyzed by BiFC assay. T87 protoplasts were transiently co-transformed with pairs of plasmids encoding: AtSCS-B-cEYFP and nEYFP-SnRK2.4 (C), AtSCS-B-cEYFP and nEYFP-SnRK2.10 (D), AtSCS-B-cEYFP and nEYFP-SnRK2.6 (E), AtSCS-B-cEYFP and nEYFP-SnRK2.8 (F). The binding led to reconstitution of functional YFP from chimeric proteins bearing non-florescent halves of YFP. For negative control, AtSCS-B-cEYFP was co-expressed with AtSCS-B-nEYFP (G). Scale bar = 10 μm; BF, bright field. The data shown here represent one of three independent experiments, all with similar results.

Figure 3.

AtSCS-A and AtSCS-B inhibit the SnRK2 activity in vitro and in vivo. AtSCS-B inhibition of SnRK2.6 (A) and SnRK2.8 (B) is calcium independent. SnRK2.6, SnRK2.8, and AtSCS-B were expressed in *E.coli* and the kinase activity was measured in the presence of increasing amounts of AtSCS-B (0, 40, 80 and 160 ng per μL) without or with Ca^{2+} (2 mM EGTA or 1 mM $CaCl_2$, respectively) in the reaction mixture. The kinase activity was monitored using MBP and [γ^{32}P]ATP as substrates. Reaction products were separated by SDS-PAGE and MBP phosphorylation was determined by autoradiography. The data represent one of three independent experiments showing similar results.

The expression of AtSCS-A and AtSCS-B in seedlings of homozygous transgenic lines 35S::AtSCS-A-c-myc (A26 and A35) and 35S::AtSCS-B-c-myc (B12 and B31) was measured at protein (C) and transcript (D) levels. The production of AtSCS-A-c-myc and AtSCS-B-c-myc proteins was monitored in seedlings of the transgenic plants by Western blotting using anti-c-myc antibodies. *AtSCS* mRNA level was monitored in the transgenic plants expressing *AtSCS-A-c-myc* or *AtSCS-B-c-myc*, or *c-myc* (vector control: P1, P17), the *scs-1* and *scs-2* mutants, as well in the WT plants by quantitative RT-PCR analysis. Data represent means of triplicate biological repeats, and the error bars indicate SD.

Analysis of the SnRK2 activity in 2-week-old seedlings of the WT, transgenic plants expressing *AtSCS-A-c-myc* or *AtSCS-B-c-myc*, and selected *snrk2* knockout mutants subjected to 100 μM ABA (E) or 350 mM NaCl (F) shows significant *in planta*

inhibition by AtSCS isoforms. The kinase activity was monitored by in-gel-kinase activity assay using as substrate GST-ABF2 (G73-Q120) or MBP, respectively. The representative results from one of three independent experiments are shown.

Figure 4.

AtSCS-A and AtSCS-B Regulate the Response of Arabidopsis to Water Deficit. The drought survival rate test (A). The Arabidopsis plants were grown in pots for 17 days under long day conditions and for an additional 2 weeks without watering. The pictures were taken before watering was stopped (before drought), after two weeks without water (drought), and two days after re-watering (re-watering). Ten pots with approximately 50 plants per pot for each line per experiment were used. Representative plants are presented. The drought survival rate (B) was estimated by analysis of at least 1000 plants per each line. For the statistical analysis a t-test was applied. The asterisks indicate significant differences from the wild type (*P < 0.05; **P < 0.01, ***P < 0.001). The average values ± SE are shown.

Water loss from detached Arabidopsis rosettes (C). Rates of water loss from the whole rosettes of six-week-old plants of wild type and different mutant lines were measured at the time points indicated. Finally, the rosettes were dried at 70°C overnight and weighed. The cut rosette water loss (CRWL) was calculated. The representative results from one of four independent experiments are shown. Eight plants were used for each line per experiment. For the statistical analysis, a t-test was applied. The asterisks indicate significant differences from the wild type (*P < 0.05; **P < 0.01, ***P < 0.001). The average values ± SE are shown.

Figure 5.

AtSCS-B Binds Ca2+ Without a Substantial Effect on the Protein Conformation. The fluorescence spectra of AtSCS-B and AtSCS-A proteins (A). The fluorescence spectra of 1.2 μM solution of AtSCS-A or AtSCS-B protein, excited at 280nm (upper curves) or at 295nm (bottom curves). apo AtSCS-A protein (blue line), apo AtSCS-B protein (black line), holo AtSCS-A (magenta line), and holo AtSCS-B (green line) are presented. The fluorescence spectra represent one of three independent measurements.

The fluorescence titration curves of AtSCS-B protein by calcium ions (B). The fluorescence excitation and the emission were at 280 and 342 nm (open triangles) or

280 and 340 nm (black circles, open squares), respectively. The calcium ions titration of 1.5 μM solutions of AtSCS-B as well as the experimental errors and the theoretical curves, calculated for a single-site ligand binding model (solid lines), are shown.

Conformational changes of AtSCS-A and AtSCS-B proteins upon Ca^{2+}binding. (C) CD spectra of 2 μM solutions of AtSCS-B or AtSCS-A with 1 mM Ca^{2+} (green and magenta lines, respectively) or without Ca^{2+} (100 μM EDTA; blue for apo AtSCS-A and black for apo-AtSCS-B).

Changes of conformational dynamics of AtSCS-A and AtSCS-B upon Ca^{2+} binding. (D) H/D exchange in AtSCS-A (left panels) and AtSCS-B (right panels) in the presence (magenta) or in the absence of Ca^{2+} (EGTA, blue). The proteins were incubated in D_2O buffer for various times (10 sec, 1 min, 20 min, 60 min) and the extent of H/D exchange was determined by mass spectrometry. The horizontal red and blue bars indicate individual peptides identified by mass spectrometry. The X-axis indicates their position in the amino acid sequence of the AtSCS-A. The Y-axis shows relative deuterium uptake calculated as described in Material and Methods; the value 1 represents maximal deuteration level, meaning that all hydrogens in amide bonds of particular peptide were exchanged to deuterium. Error bars are standard deviations from at least three independent experiments. Dark grey – position of calcium binding loops of the canonical EF-hand motif, light grey – positions calcium binding loops of potential non-canonical EF-hand motifs.

Figure 6.

Modeled by homology structures of N-terminal (residues 26-175) (A) and C-terminal (residues 251-330) (B) parts of AtSCS-A The ribbon representation follows the protein backbone. In magenta and blue are marked peptides predicted as canonical or non-canonical, respectively, EF-hand calcium binding loops. Residues putatively involved in calcium binding are denoted by sticks, yellow spheres represent calcium ions. Tyrosine residues are labeled by orange color.

Supplemental Data

Supplemental Table S1.

List of primers.

Supplemental Figure S1.

AtSCS-A *and* AtSCS-B *transcript levels in different organs.*

Different presentation of data showed in Fig.1.

Supplemental Figure S2

AtSCS-A-c-myc and AtSCS-B-c-myc protein level in homozygous 35S::AtSCS-A-c-myc and 35S::AtSCS-B-c-myc transgenic plants. The level of AtSCS-A-c-myc and AtSCS-B-c-myc was analyzed by Western blotting using anti-c-myc antibodies, as described in Materials and Methods.

Supplemental Figure S3.

Analysis of expression of Rab18 *and* RD29B *in Arabidopsis plants with different level of AtSCS-A and AtSCS-B.* The relative transcript level of *RAB18* and *RD29B* in RNA extracted from 2-week-old seedlings that were either mock or 10 μM ABA-treated for 3 h was analyzed by quantitative RT-PCR

Supplemental Figure S4.

The stoichiometry of the binding of calcium ions to AtSCS-B. The index n equal to 1 was calculated based on the general equation describing the association of the ligand to the protein used for the analysis of the fluorescence measurements. The squares and the rings describe the data from two independent experiments.

Supplemental Figure S5.

Differences in the Hydrogen/Deuterium (H/D) exchange pattern in AtSCS-A and AtSCS-B upon Ca^{2+} *binding.* Differential plot of H/D exchange presented in Fig. 8. Δ Fraction Exchanged was calculated by subtracting Fraction Exchanged values in peptides of AtSCS-A (left panels) and AtSCS-B (right panels) in the presence and absence of calcium. Peptides with p-values below 0.01 in the t-test are labeled in bright purple. Dark grey – position of calcium binding loops of the canonical EF-hand motif, light grey – positions of calcium binding loops of potential non-canonical EF-hand motifs.

Supplemental Figure S6.

Differences in the Hydrogen/Deuterium (H/D) exchange pattern between AtSCS-A and AtSCS-B in common regions in the presence and absence of calcium ions. Δ Fraction Exchanged was calculated by subtracting Fraction Exchanged values in the same peptides of AtSCS-A and AtSCS-B in the presence and absence of calcium, respectively (samples are the same as presented in Fig. 8). Peptides with p-values below 0.01 in the t-test are labeled in bright purple. Light grey – positions of calcium binding loops of potential non-canonical EF-hand motifs.

Supplemental Figure S7.

Kinetics of H/D exchange in AtSCS-A and AtSCS-B in the presence or absence of Ca^{2+}. Kinetics of H/D exchange in the presence of Ca^{2+} (magenta lines for AtSCS-A, green lines for AtSCS-B) and in the absence of Ca^{2+} (blue lines for AtSCS-A, black lines for AtSCS-B) for peptides resulting from AtSCS-A fragments starting from residue 2 to residue 81 (A), from AtSCS-A and AtSCS-B fragments from residues 85 to 160 (B), from AtSCS-A and AtSCS-B fragments from 148 to 255 (C), and from AtSCS-A and AtSCS-B fragments from 245 to 375 (D). H/D exchange was analyzed at four time points plotted on a logarithmic scale. Time in minutes (10 sec, 1 min, 20 min, 60 min) is shown at the top of the graph. Error bars represent standard deviations calculated from at least three independent experiments.

Supplemental Figure S8.

Model of N-terminal domain of AtSCS-A (region 16-119) (A) and C-terminal domain of AtSCS-A and AtSCS-B (region 241-339) (B) with overlaid H/D exchange results. Regions with relatively high H/D exchange (exchange fraction higher than 0.5 after 1 min incubation with D_2O in the presence of Ca^{2+}) are marked with yellow, regions with retarded H/D exchange (exchange fraction lower than 0.5 after 1 min incubation with D_2O in the presence of Ca^{2+}) are marked with purple. For AtSCS-A kinetics of H/D exchange is presented in the presence (red) and absence of Ca^{2+} (blue) (A) and (B), for AtSCS-B in the presence of Ca^{2+} (green) and absence of Ca^{2+} (black) (B).

Parsed Citations

Batistič O, Kudla J (2009) Plant calcineurin B-like proteins and their interacting protein kinases. Biochim Biophys Acta - Mol Cell Res 1793: 985–992
Pubmed: Author and Title
Google Scholar: Author Only Title Only Author and Title

Batistič O, Kudla J (2012) Analysis of calcium signaling pathways in plants. Biochim Biophys Acta - Gen Subj 1820: 1283–1293
Pubmed: Author and Title
Google Scholar: Author Only Title Only Author and Title

Bouchabke O, Chang F, Simon M, Voisin R, Pelletier G, Durand-Tardif M (2008) Natural variation in Arabidopsis thaliana as a tool for highlighting differential drought responses. PLoS One. Feb 27;3(2):e1705
Pubmed: Author and Title
Google Scholar: Author Only Title Only Author and Title

Böhm G, Muhr R, Jaenicke R (1992) Quantitative analysis of protein far UV circular dichroism spectra by neural networks. Protein Eng 5: 191–195
Pubmed: Author and Title
Google Scholar: Author Only Title Only Author and Title

Brandt B, Brodsky DE, Xue S, Negi J, Iba K, Kangasjärvi J, Ghassemian M, Stephan AB, Hu H, Schroeder JI (2012) Reconstitution of abscisic acid activation of SLAC1 anion channel by CPK6 and OST1 kinases and branched ABI1 PP2C phosphatase action. Proc Natl Acad Sci U S A 109:10593-10598
Pubmed: Author and Title
Google Scholar: Author Only Title Only Author and Title

Brandt B, Munemasa S, Wang C, Nguyen D, Yong T, Yang PG, Poretsky E, Belknap TF, Waadt R, Alemán F, Schroeder JI (2015) Calcium specificity signaling mechanisms in abscisic acid signal transduction in Arabidopsis guard cells. eLife 4:e03599, and erratum (2015) 4:e10328.
Pubmed: Author and Title
Google Scholar: Author Only Title Only Author and Title

Bucholc M, Ciesielski A, Goch G, Anielska-Mazur A, Kulik A, Krzywińska E, Dobrowolska G (2011) SNF1-related protein kinases 2 are negatively regulated by a plant-specific calcium sensor. J Biol Chem 286: 3429–41
Pubmed: Author and Title
Google Scholar: Author Only Title Only Author and Title

Clough SJ, Bent AF (1998) Floral dip: a simplified method for Agrobacterium-mediated transformation of Arabidopsis thaliana. Plant J 16: 735-43
Pubmed: Author and Title
Google Scholar: Author Only Title Only Author and Title

Day IS, Reddy VS, Shad Ali G, Reddy AS (2002) Analysis of EF-hand-containing proteins in Arabidopsis. Genome Biol 3: RESEARCH0056.
Pubmed: Author and Title
Google Scholar: Author Only Title Only Author and Title

Eftink MR (1997) Fluorescence methods for studying equilibrium macromolecule-ligand interactions. Methods Enzymol 278: 221–257
Pubmed: Author and Title
Google Scholar: Author Only Title Only Author and Title

Fujii H, Verslues PE, Zhu J-K (2007) Identification of two protein kinases required for abscisic acid regulation of seed germination, root growth, and gene expression in Arabidopsis. Plant Cell 19: 485–94
Pubmed: Author and Title
Google Scholar: Author Only Title Only Author and Title

Fujii H, Verslues PE, Zhu JK (2011) Arabidopsis decuple mutant reveals the importance of SnRK2 kinases in osmotic stress responses in vivo. Proc Natl Acad Sci U S A 108: 1717-1722
Pubmed: Author and Title
Google Scholar: Author Only Title Only Author and Title

Fujii H, Zhu J-K (2009) Arabidopsis mutant deficient in 3 abscisic acid-activated protein kinases reveals critical roles in growth, reproduction, and stress. Proc Natl Acad Sci U S A 106: 8380–8385
Pubmed: Author and Title
Google Scholar: Author Only Title Only Author and Title

Fujita Y, Fujita M, Shinozaki K, Yamaguchi-Shinozaki K (2011) ABA-mediated transcriptional regulation in response to osmotic stress in plants. J Plant Res 124: 509–525
Pubmed: Author and Title
Google Scholar: Author Only Title Only Author and Title

Fujita Y, Nakashima K, Yoshida T, Katagiri T, Kidokoro S, Kanamori N, Umezawa T, Fujita M, Maruyama K, Ishiyama K, et al (2009) Three SnRK2 protein kinases are the main positive regulators of abscisic acid signaling in response to water stress in Arabidopsis. Plant Cell

Physiol 50: 2123–2132
Pubmed: Author and Title
Google Scholar: Author Only Title Only Author and Title

Geiger D, Scherzer S, Mumm P, Marten I, Ache P, Matschi S, Liese A, Wellmann C, Al-Rasheid KA, Grill E, Romeis T, Hedrich R (2010) Guard cell anion channel SLAC1 is regulated by CDPK protein kinases with distinct Ca2+ affinities. Proc Natl Acad Sci U S A. 107: 8023-8028
Pubmed: Author and Title
Google Scholar: Author Only Title Only Author and Title

Halling DB, Lebeskind BJ, Hall AW, Aldrich RW (2016) Conserved properties of individual Ca2+-binding sites in calmodulin. Proc Natl Acad Sci U S A 113(9): E1216-1225
Pubmed: Author and Title
Google Scholar: Author Only Title Only Author and Title

Han JP, Köster P, Drerup MM, Scholz M, Li S, Edel KH, Hashimoto K, Kuchitsu K, Hippler M, Kudla J (2019) New Phytol 221:1935-1949
Pubmed: Author and Title
Google Scholar: Author Only Title Only Author and Title

Harmon AC (2003) Calcium-regulated protein kinases of plants. Gravitational Sp Biol Bull 16: 83–90
Pubmed: Author and Title
Google Scholar: Author Only Title Only Author and Title

Holappa LD, Ronald PC, Kramer EM (2017) Evolutionary Analysis of Snf1-Related Protein Kinase2 (SnRK2) and Calcium Sensor (SCS) Gene Lineages, and Dimerization of Rice Homologs, Suggest Deep Biochemical Conservation across Angiosperms. Front Plant Sci 8:395
Pubmed: Author and Title
Google Scholar: Author Only Title Only Author and Title

Hou Y-J, Zhu Y, Wang P, Zhao Y, Xie S, Batelli G, Wang B, Duan C-G, Wang X, Xing L, et al (2016) Type One Protein Phosphatase 1 and Its Regulatory Protein Inhibitor 2 Negatively Regulate ABA Signaling. PLoS Genet. doi: 10.1371/journal.pgen.1005835
Pubmed: Author and Title
Google Scholar: Author Only Title Only Author and Title

Hubbard KE, Nishimura N, Hitomi K, Getzoff ED, Schroeder JI (2010) Early abscisic acid signal transduction mechanisms: Newly discovered components and newly emerging questions. Genes Dev 24: 1695–1708
Pubmed: Author and Title
Google Scholar: Author Only Title Only Author and Title

De Klerk E, 't Hoen PA (2015) Alternative mRNA transcription, processing, and translation: insights from RNA sequencing. Trends Genet 31: 128–139
Pubmed: Author and Title
Google Scholar: Author Only Title Only Author and Title

Komatsu K, Suzuki N, Kuwamura M, Nishikawa Y, Nakatani M, Ohtawa H, Takezawa D, Seki M, Tanaka M, Taji T, Hayashi T, Sakata Y (2013) Group A PP2Cs evolved in land plants as key regulators of intrinsic desiccation tolerance. Nat Commun 4:2219.
Pubmed: Author and Title
Google Scholar: Author Only Title Only Author and Title

Krieger E, Joo K, Lee J, Lee J, Raman S, Thompson J, Tyka M, Baker D, Karplus K (2009) Improving physical realism, stereochemistry, and side-chain accuracy in homology modeling: Four approaches that performed well in CASP8. Proteins 77 Suppl 9: 114–122
Pubmed: Author and Title
Google Scholar: Author Only Title Only Author and Title

Krieger E, Koraimann G, Vriend G (2002) Increasing the precision of comparative models with YASARA NOVA--a self-parameterizing force field. Proteins 47: 393–402
Pubmed: Author and Title
Google Scholar: Author Only Title Only Author and Title

Krzywińska E, Bucholc M, Kulik A, Ciesielski A, Lichocka M, Dębski J, Ludwików A, Dadlez M, Rodriguez PL, Dobrowolska G (2016) Phosphatase ABI1 and okadaic acid-sensitive phosphoprotein phosphatases inhibit salt stress-activated SnRK2.4 kinase. BMC Plant Biol. doi: 10.1186/s12870-016-0817-1
Pubmed: Author and Title
Google Scholar: Author Only Title Only Author and Title

Kulik A, Anielska-Mazur A, Bucholc M, Koen E, Szymanska K, Zmienko A, Krzywinska E, Wawer I, McLoughlin F, Ruszkowski D, et al (2012) SNF1-related protein kinases type 2 are involved in plant responses to cadmium stress. Plant Physiol 160: 868–883
Pubmed: Author and Title
Google Scholar: Author Only Title Only Author and Title

Kulik A, Wawer I, Krzywińska E, Bucholc M, Dobrowolska G (2011) SnRK2 Protein Kinases-Key Regulators of Plant Response to Abiotic Stresses. Omi A J Integr Biol 15: 859–872
Pubmed: Author and Title
Google Scholar: Author Only Title Only Author and Title

Luan S (2009) The CBL-CIPK network in plant calcium signaling. Trends Plant Sci 14: 37–42
Pubmed: Author and Title
Google Scholar: Author Only Title Only Author and Title

Mach H, Middaugh CR, Lewis R V (1992) Statistical determination of the average values of the extinction coefficients of tryptophan and tyrosine in native proteins. Anal Biochem 200: 74–80
Pubmed: Author and Title
Google Scholar: Author Only Title Only Author and Title

Maszkowska J, Dębski J, Kulik A, Kistowski M, Bucholc M, Lichocka M, Klimecka M, Sztatelman O, Szymańska KP, Dadlez M, Dobrowolska G (2019) Plant Cell Environ. Mar;42(3):931-946
Pubmed: Author and Title
Google Scholar: Author Only Title Only Author and Title

McLoughlin F, Galvan-Ampudia CS, Julkowska MM, Caarls L, van der Does D, Laurière C, Munnik T, Haring MA, Testerink C (2012) The Snf1-related protein kinases SnRK2.4 and SnRK2.10 are involved in maintenance of root system architecture during salt stress. Plant J 72: 436-449
Pubmed: Author and Title
Google Scholar: Author Only Title Only Author and Title

Melotto M, Underwood W, Koczan J, Nomura K, He SY (2006) Plant stomata function in innate immunity against bacterial invasion. Cell 126: 969–980
Pubmed: Author and Title
Google Scholar: Author Only Title Only Author and Title

Merilo E, Laanemets K, Hu H, Xue S, Jakobson L, Tulva I, Gonzalez-Guzman M, Rodriguez PL, Schroeder JI, Brosche M, et al (2013) PYR/RCAR receptors contribute to ozone-, reduced air humidity-, darkness-, and CO2-induced stomatal regulation. Plant Physiol 162: 1652–1668
Pubmed: Author and Title
Google Scholar: Author Only Title Only Author and Title

Mizoguchi M, Umezawa T, Nakashima K, Kidokoro S, Takasaki H, Fujita Y, Yamaguchi-Shinozaki K, Shinozaki K (2010) Two closely related subclass II SnRK2 protein kinases cooperatively regulate drought-inducible gene. Plant Cell Physiol 51: 842-847
Pubmed: Author and Title
Google Scholar: Author Only Title Only Author and Title

Mustilli A-C, Merlot S, Vavasseur A, Fenzi F, Giraudat J (2002) Arabidopsis OST1 protein kinase mediates the regulation of stomatal aperture by abscisic acid and acts upstream of reactive oxygen species production. Plant Cell 14: 3089–3099
Pubmed: Author and Title
Google Scholar: Author Only Title Only Author and Title

Nakamura S1, Mano S, Tanaka Y, Ohnishi M, Nakamori C, Araki M, Niwa T, Nishimura M, Kaminaka H, Nakagawa T, Sato Y, Ishiguro S (2010) Gateway binary vectors with the bialaphos resistance gene, bar, as a selection marker for plant transformation. Biosci Biotechnol Biochem 74:1315-1319-
Pubmed: Author and Title
Google Scholar: Author Only Title Only Author and Title

Nakashima K, Yamaguchi-Shinozaki K (2013) ABA signaling in stress-response and seed development. Plant Cell Rep 32: 959–970
Pubmed: Author and Title
Google Scholar: Author Only Title Only Author and Title

Nakashima K, Fujita Y, Kanamori N, Katagiri T, Umezawa T, Kidokoro S, Maruyama K, Yoshida T, Ishiyama K, Kobayashi M, et al (2009) Three Arabidopsis SnRK2 protein kinases, SRK2D/SnRK2.2, SRK2E/SnRK2.6/OST1 and SRK2I/SnRK2.3, involved in ABA signaling are essential for the control of seed development and dormancy. Plant Cell Physiol 50: 1345–1363
Pubmed: Author and Title
Google Scholar: Author Only Title Only Author and Title

Nelson MR, Chazin WJ (1998) Structures of EF-hand Ca2+-binding proteins: Diversity in the organization, packing and response to Ca2+ binding. BioMetals 11: 297–318
Pubmed: Author and Title
Google Scholar: Author Only Title Only Author and Title

Ng LM, Melcher K, Teh BT, Xu HE (2014) Abscisic acid perception and signaling: structural mechanisms and applications. Acta Pharmacol Sin 35: 567–584
Pubmed: Author and Title
Google Scholar: Author Only Title Only Author and Title

Reddy VS, Reddy ASN (2004) Proteomics of calcium-signaling components in plants. Phytochemistry 65: 1745–1776
Pubmed: Author and Title
Google Scholar: Author Only Title Only Author and Title

Rubio S, Rodrigues A, Saez A, Dizon MB, Galle A, Kim TH, Santiago J, Flexas J, Schroeder JI, Rodriguez PL (2009) Triple loss of function of protein phosphatases type 2C leads to partial constitutive response to endogenous abscisic acid. Plant Physiol 150:1345-1355

Pubmed: Author and Title
Google Scholar: Author Only Title Only Author and Title

Sanchez-Barrena MJ, Martinez-Ripoll M, Albert A (2013) Structural Biology of a Major Signaling Network that Regulates Plant Abiotic Stress: The CBL-CIPK Mediated Pathway. Int J Mol Sci 14: 5734–5749
Pubmed: Author and Title
Google Scholar: Author Only Title Only Author and Title

Schulz P1, Herde M, Romeis T (2013) Calcium-dependent protein kinases: hubs in plant stress signaling and development. Plant Physiol 163: 523-530
Pubmed: Author and Title
Google Scholar: Author Only Title Only Author and Title

Shinozawa A, Otake R, Takezawa D, Umezawa T, Komatsu K, Tanaka K, Amagai A, Ishikawa S, Hara Y, Kamisugi Y, Cuming AC, Hori K, Ohta H, Takahashi F, Shinozaki K, Hayashi T, Taji T, Sakata Y (2019) SnRK2 protein kinases represent an ancient system in plants for adaptation to a terrestrial environment. Nature Commun Biol. 2:30. doi: 10.1038/s42003-019-0281-1. eCollection
Pubmed: Author and Title
Google Scholar: Author Only Title Only Author and Title

Sirichandra C, Gu D, Hu HC, Davanture M, Lee S, Djaoui M, Valot B, Zivy M, Leung J, Merlot S, Kwak JM (2009) Phosphorylation of the Arabidopsis AtrbohF NADPH oxidase by OST1 protein kinase. FEBS Lett 583: 2982-2986
Pubmed: Author and Title
Google Scholar: Author Only Title Only Author and Title

Sitkiewicz E, Tarnowski K, Poznanski J, Kulma M, Dadlez M (2013) Oligomerization interface of RAGE receptor revealed by MS-monitored hydrogen deuterium exchange. PLoS One 8: e76353
Pubmed: Author and Title
Google Scholar: Author Only Title Only Author and Title

Soma F, Mogami J, Yoshida T, Abekura M, Takahashi F, Kidokoro S, Mizoi J, Shinozaki K, Yamaguchi-Shinozaki K (2017) ABA-unresponsive SnRK2 protein kinases regulate mRNA decay under osmotic stress in plants. Nat Plants 3: 16204
Pubmed: Author and Title
Google Scholar: Author Only Title Only Author and Title

Soon F-F, Ng L-M, Zhou XE, West GM, Kovach A, Tan MHE, Suino-Powell KM, He Y, Xu Y, Chalmers MJ, et al (2012) Molecular Mimicry Regulates ABA Signaling by SnRK2 Kinases and PP2C Phosphatases. Science 335: 85–88
Pubmed: Author and Title
Google Scholar: Author Only Title Only Author and Title

Tanaka T, Koyanagi KO, Itoh T (2009) Highly diversified molecular evolution of downstream transcription start sites in rice and Arabidopsis. Plant Physiol 149: 1316-1324
Pubmed: Author and Title
Google Scholar: Author Only Title Only Author and Title

Tzfira T, Tian GW, Lacroix B, Vyas S, Li J, Leitner-Dagan Y, Krichevsky A, Taylor T, Vainstein A, Citovsky V (2005) pSAT vectors: a modular series of plasmids for autofluorescent protein tagging and expression of multiple genes in plants. Plant Mol Biol 57: 503-516
Pubmed: Author and Title
Google Scholar: Author Only Title Only Author and Title

Umezawa T, Yoshida R, Maruyama K, Yamaguchi-Shinozaki K, Shinozaki K (2004) SRK2C, a SNF1-related protein kinase 2, improves drought tolerance by controlling stress-responsive gene expression in Arabidopsis thaliana. Proc Natl Acad Sci U S A 101:17306-17311
Pubmed: Author and Title
Google Scholar: Author Only Title Only Author and Title

Umezawa T, Sugiyama N, Mizoguchi M, Hayashi S, Myouga F, Yamaguchi-Shinozaki K, Ishihama Y, Hirayama T, Shinozaki K (2009) Type 2C protein phosphatases directly regulate abscisic acid-activated protein kinases in Arabidopsis. Proc Natl Acad Sci U S A 106: 17588–17593
Pubmed: Author and Title
Google Scholar: Author Only Title Only Author and Title

Umezawa T, Nakashima K, Miyakawa T, Kuromori T, Tanokura M, Shinozaki K, Yamaguchi-Shinozaki K (2010) Molecular basis of the core regulatory network in ABA responses: sensing, signaling and transport. Plant Cell Physiol 51:1821-1839
Pubmed: Author and Title
Google Scholar: Author Only Title Only Author and Title

Vlad F, Rubio S, Rodrigues A, Sirichandra C, Belin C, Robert N, Leung J, Rodriguez PL, Laurière C, Merlot S (2009) Protein Phosphatases 2C Regulate the Activation of the Snf1-Related Kinase OST1 by Abscisic Acid in Arabidopsis. Plant Cell 21: 3170–3184
Pubmed: Author and Title
Google Scholar: Author Only Title Only Author and Title

Wang P, Zhu JK (2016) Assessing Kinase Activity in Plants with In-Gel Kinase Assays. Methods Mol Biol 1363: 189-197
Pubmed: Author and Title
Google Scholar: Author Only Title Only Author and Title

Yamada H, Koizumi N, Nakamichi N, Kiba T, Yamashino T, Mizuno T (2004) Rapid response of Arabidopsis T87 cultured cells to

cytokinin through His-to-Asp phosphorelay signal transduction. Biosci Biotechnol Biochem 68: 1966–1976
Pubmed: Author and Title
Google Scholar: Author Only Title Only Author and Title

Yoshida R, Hobo T, Ichimura K, Mizoguchi T, Takahashi F, Aronso J, Ecker JR, Shinozaki K (2002) ABA-activated SnRK2 protein kinase is required for dehydration stress signaling in Arabidopsis. Plant Cell Physiol 43: 1473–1483
Pubmed: Author and Title
Google Scholar: Author Only Title Only Author and Title

Yoshida T, Mogami J, Yamaguchi-Shinozaki K (2015) Omics Approaches Toward Defining the Comprehensive Abscisic Acid Signaling Network in Plants. Plant Cell Physiol 56:1043-1052.
Pubmed: Author and Title
Google Scholar: Author Only Title Only Author and Title

Zhang X, Henriques R, Lin SS, Niu QW, Chua NH (2006) Agrobacterium-mediated transformation of Arabidopsis thaliana using the floral dip method. Nat Protoc 1(2): 641-646
Pubmed: Author and Title
Google Scholar: Author Only Title Only Author and Title

Zhou XE, Soon F-F, Ng L-M, Kovach A, Suino-Powell KM, Li J, Yong E-L, Zhu J-K, Xu HE, Melcher K (2012) Catalytic mechanism and kinase interactions of ABA-signaling PP2C phosphatases. Plant Signal Behav 7: 581–588
Pubmed: Author and Title
Google Scholar: Author Only Title Only Author and Title